

Localisation in 2+1 dimensional SU(3) pure gauge theory at finite temperature

Matteo Giordano^a

^a*ELTE Eötvös Loránd University, Institute for Theoretical Physics, Pázmány P. s. 1/A, H-1117, Budapest, Hungary , and
MTA-ELTE Lendület Lattice Gauge Theory Research Group, Pázmány P. s. 1/A, H-1117, Budapest, Hungary*

E-mail: giordano@bodri.elte.hu

ABSTRACT: I study the localisation properties of low Dirac eigenmodes in 2+1 dimensional SU(3) pure gauge theory, both in the low-temperature, confined and chirally-broken phase and in the high-temperature, deconfined and chirally-restored phase, by means of numerical lattice simulations. While these modes are delocalised at low temperature, they become localised at high temperature, up to a critical point in the Dirac spectrum where a BKT-type Anderson transition takes place. All results point to localisation appearing at the deconfinement temperature, and support previous expectations about the close relation between deconfinement, chiral symmetry breaking, and localisation.

KEYWORDS: Lattice Quantum Field Theory, Random Systems

Contents

1	Introduction	1
2	Localisation in lattice gauge theories	4
3	Lattice SU(3) pure gauge theory in 2+1 dimensions	7
4	Numerical results	9
4.1	Participation ratio	10
4.2	Spectral statistics	16
5	Conclusions and outlook	28

1 Introduction

The close connection between deconfinement and chiral symmetry restoration is an aspect of the finite-temperature transition in QCD that is still poorly understood. As is well known, both the confining and the chiral properties of QCD at vanishing chemical potential change dramatically in the temperature range $T \simeq 145\text{--}165$ MeV: while in the low-temperature phase quarks and gluons are confined within hadrons and chiral symmetry is spontaneously broken, in the high-temperature phase quarks and gluons are liberated into a plasma, and chiral symmetry is restored. Of course, both the spontaneous breaking and the restoration of chiral symmetry should be understood here as approximate, since chiral symmetry is explicitly (albeit softly) broken by the quark masses. Since the transition is an analytic crossover [1], there is no uniquely defined critical temperature. However, defining a pseudocritical temperature T_χ for the chiral transition as the position of the peak of the chiral susceptibility, and a pseudocritical temperature T_{dec} for the deconfinement transition as the position of the peak of the quark entropy, one finds that they agree within errors, $T_\chi = T_{\text{dec}} = T_c \approx 155$ MeV [2].

This relation between these two seemingly unrelated phenomena is not unique to QCD, but it appears quite generally in a variety of gauge theories. In particular, T_χ and T_{dec} coincide in certain theories and models where the finite-temperature transition is a genuine phase transition. Examples are provided by SU(3) pure gauge theory in 3+1 [3] and 2+1 dimensions [4],¹ and $N_f = 3$ QCD with unimproved rooted staggered fermions on $N_t = 4$ lattices [5–7]. Recent studies indicate that it is so also for the $\mathcal{N} = 1$ SU(2) super-Yang-Mills theory [8]. Another interesting case is that of 3+1 dimensional SU(3) gauge theory

¹Although, strictly speaking, there is no chiral symmetry here since there are no fermions, one can nevertheless define a valence chiral condensate and study its behaviour in the limit of vanishing valence quark mass.

with $N_f = 2$ flavours of adjoint fermions [9] on the lattice:² here two phase transitions are present, a deconfining one at T_{dec} and a chiral-symmetry-restoring one at T_χ with $T_{\text{dec}} < T_\chi$. Nonetheless, at T_{dec} the chiral condensate jumps downwards, and a partial restoration of chiral symmetry happens via a first-order phase transition.

It is also well known that the fate of chiral symmetry is determined by the spectrum of the Dirac operator near the origin. In fact, the celebrated Banks-Casher relation [11] establishes that the chiral condensate in the chiral limit is proportional to the spectral density of the Dirac operator near the origin. For finite but small quark masses, an accumulation of eigenmodes near the origin is still expected at low temperatures, leading to light pions and all the other phenomenological consequences for QCD due to its being close to a theory with spontaneously broken symmetry. At high temperatures, instead, the spectral density is expected to vanish near the origin, reflecting the restoration of chiral symmetry in the massless case. Given the close relation between confining and chiral properties of the theory, it is natural to wonder if confinement is somehow responsible for the accumulation of modes near the origin, and analogously if deconfinement causes the depletion of this spectral region. A similar question of course can be asked also for other gauge theories.

Adding to the mystery, or possibly helping to solve it, a third phenomenon has been observed to take place in QCD around the critical temperature, namely the localisation of the lowest modes of the Dirac operator [12–18]. Numerical studies on the lattice have shown that while in the low-temperature phase all the Dirac modes are extended throughout the whole system, above T_c the lowest modes get localised [12–18] on the scale of the inverse temperature [16]. More precisely, modes are localised up to a temperature-dependent critical point in the spectrum, $\lambda_c = \lambda_c(T)$.³ At λ_c , a second-order phase transition takes place in the spectrum [19], and modes become delocalised. This type of transitions is well known in the condensed-matter literature as *Anderson transitions* [20, 21], and the corresponding critical point is known as *mobility edge*. The mobility edge, λ_c , vanishes at a temperature compatible with T_c [16], suggesting that localisation of the low Dirac modes is closely related to deconfinement and chiral restoration. This is further supported by a similar coincidence of the three phenomena in other theories and models, like SU(3) pure gauge theory in 3+1 dimensions [22], the $N_f = 3$ unimproved staggered fermion model mentioned above [23], and also in a toy model for QCD [24], devised in Ref. [25] precisely to study the issue of localisation.

A qualitative understanding of the relation between deconfinement and localisation is provided by what in this paper will be referred to as the “sea/islands” picture of localisation [26, 27]. The idea is that the local Polyakov lines provide a sort of local potential for the Dirac modes via the effective boundary condition that they impose on the eigenmodes. In the high-temperature phase, this looks like a “sea” corresponding to the Polyakov lines

²The continuum theory might lie inside the conformal window, but numerical studies have been inconclusive so far [10].

³Here and in the following, with a slight abuse of terminology, I will call “eigenvalue” what is really the imaginary part of the eigenvalue.

ordered along the identity, in which “islands” corresponding to non-aligned Polyakov lines appear. Such islands are “energetically” favourable, and thus provide convenient places where the eigenmodes can localise. This picture is made more precise by exactly recasting the staggered Dirac operator as the Hamiltonian of a set of coupled three-dimensional Anderson models [25], with the phases of the local Polyakov lines acting as the source of a random on-site potential, and with the strength of the coupling among the different Anderson models decreasing as the system gets ordered. Notice that the dimensionality of the relevant Anderson models matches the spatial dimension of the gauge theory. The “Dirac-Anderson” form of the staggered operator suggests that the strength of the coupling plays an important role for the fate of localisation, as well as for the spontaneous breaking of chiral symmetry: as the Anderson models decouple, it becomes more difficult for modes to accumulate around the origin. These ideas are supported by the results of a detailed study on variations of a toy model for QCD [25].

An interesting aspect of the sea/islands picture and of the Dirac-Anderson approach to localisation and chiral symmetry restoration is that they depend only marginally on the dimensionality of the system, or the gauge group, or the type of fermions present in the theory: all that is required for the argument to apply is essentially the existence of an ordered phase with Polyakov lines aligning to the identity, and the possibility for modes to localise in the relevant Anderson model. A non trivial test of these ideas can then be performed by studying gauge theories in different dimensions, with different gauge groups, and different fermion representations. In this paper we try the first possibility, studying SU(3) pure gauge theory in 2+1 dimensions on the lattice using staggered fermions. As already mentioned above, this theory is known to display a deconfining and chiral-symmetry-restoring second-order phase transition at finite temperature.

The choice of dimensionality is somewhat peculiar, both for chiral symmetry and localisation. As a matter of fact, chiral symmetry as usually defined does not even exist in odd dimensions. However, in three dimensions for an even number of flavours, N_f , it is possible to reorganise the N_f two-component spinors into $N_f/2$ four-component spinors, and in the massless case the continuum Dirac action is invariant under a $U(N_f)$ flavour symmetry group with two “chiral” subgroups [28, 29].⁴ While these are explicitly broken by a mass term, in the massless case one can meaningfully ask if they are spontaneously broken due to the formation of a quark-antiquark condensate, which breaks the flavour symmetry down to $U(1) \times U(1) \times SU(N_f/2) \times SU(N_f/2)$ [28]. The Banks-Casher relation then ties the spontaneous breaking of this symmetry to the accumulation of Dirac eigenmodes around zero. Concerning localisation, in two dimensions the existence of an Anderson transition from localised to delocalised modes in a disordered system depends on the details of the model (see, e.g., Ref. [21]). Using one flavour of staggered fermions, one has effectively $N_f = 2$ in the continuum due to the doubling phenomenon, so that chiral symmetry (in the above sense) can

⁴This construction generalises to any odd dimension D , reorganising the N_f $2^{\frac{D-1}{2}}$ -component spinors into $\frac{N_f}{2}$ $2^{\frac{D+1}{2}}$ -component spinors [29].

be defined; using $SU(3)$ as gauge group, the symmetry class in the classification of Random Matrix Theory is the unitary one, for which Anderson transitions in two spatial dimensions are known to exist [30].

As there is no obstruction to the sea/islands picture to work, then it should just work, leading to the same situation encountered in 3+1 dimensions: at low temperature, chiral symmetry should be spontaneously broken by the accumulation of delocalised Dirac eigenmodes near the origin; at high temperature, the spectral density should vanish near the origin, leading to chiral symmetry restoration, and modes should be localised up to a mobility edge somewhere in the spectrum. It is already known that chiral symmetry is restored at deconfinement [4]. It is the purpose of this work to verify that the localisation properties of the low modes change there as well.

The plan of this paper is the following. In Section 2 I briefly review localisation in disordered systems, with a special focus on lattice gauge theories in 3+1 dimensions. In Section 3 I describe in some detail the specific model under consideration, and expectations about its behaviour. In Section 4 I show numerical results and their analysis. Conclusions and perspectives on future investigations are discussed in Section 5.

2 Localisation in lattice gauge theories

Localisation is a well known phenomenon in condensed matter physics. It has long been known, since the seminal work of Anderson [31], that the addition of a random on-site potential to the usual tight-binding Hamiltonian causes the localisation of the energy states at the band edge, beyond a critical energy E_c called mobility edge, while states in the band centre remain extended (see Ref. [20] for a review). Such “disordered Hamiltonians” aim at describing metals with impurities, and in this context the width W of the distribution of the on-site potential is a measure of the amount of impurities in the system. As the disorder parameter W is increased, the mobility edge moves towards the band centre, and all modes become localised beyond some critical disorder, turning the metal into an insulator. In three (and higher) dimensions the transition between localised and delocalised modes is a second-order quantum phase transition known as Anderson transition (see Ref. [21] for a review), with a divergent correlation length $\xi \sim |E - E_c|^{-\nu}$ characterised by the critical exponent ν .

Localisation in gauge theories was initially studied at zero temperature in investigations of the topological structure of the QCD vacuum (see the review Ref. [32] and references therein). The idea that the finite-temperature transition of QCD could be related to localisation of the low Dirac modes dates back to Refs. [33–35]. The first numerical results supporting this idea appeared in Ref. [12], coming from the effective description of QCD via an Instanton Liquid Model, and in Ref. [13], coming from numerical simulations of QCD on a lattice, both in the quenched approximation and with 2+1 flavours of staggered fermions. Further evidence of localisation of the low Dirac modes in the high-temperature phase of QCD was provided by the absence of correlations in the low-lying spectrum of the overlap operator [14], typical of localised modes.

A detailed study of localisation in lattice QCD was undertaken in Ref. [16], using 2+1 flavours of 2-stout improved rooted staggered fermions. There, it was shown that above T_c the eigenmodes of the staggered Dirac operator are localised, for (imaginary part of the) eigenvalue up to a temperature-dependent mobility edge, $\lambda_c(T)$, beyond which modes become extended. The extrapolation of $\lambda_c(T)$ vanishes at a temperature compatible with T_c , in agreement with the absence of localised modes in the low-temperature phase. Localisation was shown to survive the continuum limit, indicating that it is not a lattice artefact. This is also supported by the fact that localised modes have been found with other fermion discretisations, namely with domain-wall fermions [17] and with overlap fermions on twisted-mass Wilson fermion backgrounds [18].

Localisation in the high-temperature, deconfined phase has been observed also in other gauge theories (see Ref. [36] for a recent review), namely SU(2) [15] and SU(3) pure gauge theory [22], and SU(3) with $N_f = 3$ flavours of unimproved rooted staggered fermions on $N_t = 4$ lattices [23]. In these models the finite-temperature transition is a genuine phase transition, which provides a clean-cut setting for investigating the possible coincidence of deconfinement, chiral-symmetry restoration and localisation of the low Dirac modes. While in the first case a detailed study of the temperature dependence of the mobility edge is missing, in the other two cases it was indeed found that the low Dirac modes start localising precisely at the critical temperature where deconfinement and chiral-symmetry restoration take place. A similar result was found in a toy model for QCD [24], where the Polyakov-line dynamics is mimicked by a spin model: as the spins get ordered, the low Dirac modes localise and their density near the origin drops to zero.

The simplest way to identify localised modes is by studying their so-called *participation ratio* (PR). Given a normalised eigenmode of a lattice Dirac operator, $\Psi(n)$, one defines the inverse participation ratio (IPR) as

$$\text{IPR} = \sum_n |\Psi(n)^\dagger \Psi(n)|^2, \quad (2.1)$$

where $\Psi(n)^\dagger \Psi(n)$ denotes the scalar product in colour and (possibly) Dirac space, and the sum is over the lattice sites n .⁵ The PR is just the inverse of the IPR divided by the lattice size,

$$\text{PR} = \frac{\text{IPR}^{-1}}{N_t V}, \quad V = N_s^d, \quad (2.2)$$

where we have assumed that the lattice is a $(d+1)$ -dimensional hypercube of spatial extension N_s and temporal extension N_t in lattice units. In all the models discussed above $d = 3$, while in this work I will consider $d = 2$. For a fully delocalised mode, $\Psi(n)^\dagger \Psi(n) \sim 1/V$, so that the PR remains constant in the large volume limit.⁶ For a mode localised in a spatial region of fixed size v one finds instead $\text{PR} \sim v/V \rightarrow 0$ in the large-volume limit.

⁵ We mention in passing the generalised IPRs, defined as $\text{IPR}_q \equiv \sum_n |\Psi(n)^\dagger \Psi(n)|^q$. Clearly $\text{IPR} = \text{IPR}_2$.

⁶With “volume” I will refer to the spatial volume $V = N_s^d$, unless it is explicitly stated otherwise.

A useful observation is that in a random matrix model the localisation properties of the eigenmodes and the statistical properties of the corresponding eigenvalues are closely related [37]. For localised modes the eigenvalues fluctuate independently, following Poisson statistics, while for extended modes the eigenvalue statistics are those of the appropriate Gaussian ensemble of Random Matrix Theory (RMT; see Ref. [38] for a general introduction, and Refs. [39, 40] for the application of RMT to QCD). This is made evident after unfolding the spectrum, i.e., after mapping $\lambda_i \rightarrow x_i = \int^{\lambda_i} d\lambda' \rho(\lambda')$, where $\rho(\lambda) \equiv \langle \sum_i \delta(\lambda - \lambda_i) \rangle$ is the spectral density and $\langle \dots \rangle$ denotes averaging over the random matrix ensemble. This mapping makes the spectral density identically 1 throughout the spectrum. It is well known that for dense matrices the (bulk) statistical properties of the unfolded spectrum are universal and uniform throughout the spectrum, i.e., do not depend on the details of the random matrix model under study, but only on the symmetry class of the ensemble [38]. The main classes are the orthogonal, unitary, and symplectic classes.⁷ Universal analytic results can therefore be obtained using the so-called Gaussian ensembles. In particular, the probability distribution of consecutive unfolded level spacings $s_i \equiv x_{i+1} - x_i$ is known, and very accurately approximated by the so-called *Wigner surmise*, which for the unitary class reads

$$P_{\text{RMT}}(s) = \frac{32}{\pi^2} s^2 e^{-\frac{4}{\pi} s^2} . \quad (2.3)$$

In contrast, for eigenvalues that fluctuate independently the unfolded level spacing distribution is the exponential function, appropriate for Poisson statistics,

$$P_{\text{Poisson}}(s) = e^{-s} . \quad (2.4)$$

The lattice Dirac operator in a gauge-field background is in practice a sparse random matrix, with fluctuations provided by the gauge links and ensemble averaging corresponding to integration over gauge fields with the appropriate measure. For ensembles of sparse matrices the statistical properties can depend on the spectral region under consideration, and so it is customary to compute the spectral statistics locally in the spectrum, i.e., restricting to small spectral intervals around the chosen point. Looking at Dirac spectra in the high-temperature phase of QCD one sees indeed a transition from Poisson to RMT statistics. By a finite-size scaling study of statistical spectral observables it is possible to determine precisely the location of the mobility edge and the critical exponent ν [42]. This has been used to show that the localisation/delocalisation transition in the Dirac spectrum in high-temperature lattice QCD with staggered fermions is a genuine second-order phase transition in the same universality class [19] as the three-dimensional unitary Anderson model [43]. Further support to this conclusion came from a study of the multifractal properties of eigenmodes at the mobility edge [44]. This matching can be easily understood in the light of the sea/islands picture [26, 27] and of the Dirac-Anderson approach [25], since the spatial fluctuations of the Polyakov lines precisely provide the kind of three-dimensional on-site disorder present in the

⁷The classification in symmetry classes of RMT ensembles is actually richer [41], but these ensembles suffice for our purposes.

Anderson model, while the unitary symmetry class is the one to which the staggered Dirac operator belongs.

3 Lattice SU(3) pure gauge theory in 2+1 dimensions

Finite-temperature SU(3) pure gauge theory in 2+1 dimensions has been studied on the lattice in several papers [45–52]. This theory shows a deconfining second-order phase transition at finite temperature, in the same universality class as the two-dimensional 3-colour Potts model. These works used a hypercubic lattice and the Wilson action, which up to an irrelevant additive constant reads

$$S[U] = -\frac{\beta}{3} \sum_n \sum_{\mu < \nu} \operatorname{Re} \operatorname{tr} U_{\mu\nu}(n) = -\bar{\beta} \sum_n \sum_{\mu < \nu} \operatorname{Re} \operatorname{tr} U_{\mu\nu}(n), \quad (3.1)$$

where $\bar{\beta} = \beta/3$, $U_{\mu\nu}(n)$ is the usual plaquette variable,

$$U_{\mu\nu}(n) = U_\mu(n)U_\nu(n + \hat{\mu})U_\mu(n + \hat{\nu})^\dagger U_\nu(n)^\dagger, \quad (3.2)$$

$\mu, \nu = 1, 2, 3$ are the lattice directions, $U_\mu(n)$ are SU(3) gauge links living on the lattice edges $(n, n + \hat{\mu})$, and $\hat{\mu}$ denotes the unit vector in direction μ . Periodic boundary conditions both in the temporal and in the spatial directions are imposed. In 2+1 dimensions the gauge coupling g has dimensions of $[\text{mass}]^{\frac{1}{2}}$, and the lattice coupling β is related to g and the lattice spacing as $\beta = 6/(g^2 a)$.⁸ The partition function is

$$Z = \int \mathcal{D}U e^{-S[U]}, \quad \mathcal{D}U = \prod_{n,\mu} dU_\mu(n), \quad (3.3)$$

with $dU_\mu(n)$ the SU(3) Haar measure. The critical temperature was determined precisely in Ref. [49], and for lattices of temporal extension $N_t = 4$ it corresponds to the lattice gauge coupling $\bar{\beta}_c = 4.9057(57)$.

Chiral symmetry breaking, as discussed in the Introduction, was first studied in Ref. [4] with staggered fermions in the quenched approximation, so studying the Dirac operator on pure-gauge theory backgrounds. The staggered Dirac operator reads

$$D_{n,n'}^{\text{stag}} = \frac{1}{2} \sum_{\mu} \eta_{\mu}(n) \left(U_{\mu}(n) \delta_{n+\hat{\mu},n'} - U_{\mu}(n - \hat{\mu})^\dagger \delta_{n-\hat{\mu},n'} \right), \quad \eta_{\mu}(n) = (-1)^{\sum_{\nu < \mu} n_{\nu}}, \quad (3.4)$$

with periodic boundary conditions in the spatial directions and antiperiodic boundary conditions in the temporal direction, and in the continuum limit it describes $N_f = 2$ degenerate species of fermions. The staggered operator D^{stag} has purely imaginary eigenvalues, $i\lambda$, and since its spectrum is symmetric about zero it is enough to consider only $\lambda \geq 0$. Fermions break the centre symmetry of the pure-gauge theory, selecting the vacuum with trivial Polyakov lines, but when working in the quenched approximation this has to be done by hand, for

⁸For the sake of simplicity we ignore scaling violations.

example by multiplying all the temporal links in the last time slice by the appropriate centre element. This was the approach adopted in Ref. [4], which we will also use when needed. While the full chiral subgroup of the $U(N_f)$ flavour symmetry discussed in the Introduction is explicitly broken at finite lattice spacing, a remnant $U(1) \times U(1)$ chiral symmetry still survives [29], and can be spontaneously broken by the formation of a quark-antiquark condensate. The authors of Ref. [4] observed that while in the low β (low temperature), confined phase a finite chiral condensate was found in the limit of vanishing valence quark mass, this vanished in the high β , deconfined phase, and that the chiral transition coincided with the deconfinement transition.

The purpose of this work is to study the localisation properties of the low Dirac modes in the two phases of the theory, both by measuring the PR of the eigenmodes, Eq. (2.2), and by studying the statistical properties of the unfolded spectrum. After obtaining the Dirac spectra for an ensemble of gauge configurations, unfolding is done by sorting all the eigenvalues (for a given coupling and lattice size) by increasing size, and replacing them by their rank divided by the number of configurations. This automatically makes the spectral density equal to 1 throughout the spectrum. I use two quantities extracted from the unfolded level spacing distribution measured locally in the spectrum, $P_\lambda(s)$. One of them is the integrated distribution I_λ ,

$$I_\lambda = \int_0^{s_0} ds P_\lambda(s), \quad (3.5)$$

where $s_0 \simeq 0.508$ is conveniently chosen to be the crossing point of the unitary Wigner surmise, Eq. (2.3), and the exponential function, Eq. (2.4), i.e., to a very good approximation, the crossing point of the unfolded level spacing distributions for RMT and Poisson statistics. This maximises the difference between the two types of behaviour. The analytic predictions for I_λ in the two cases are $I_{\text{RMT}} \simeq 0.117$ and $I_{\text{Poisson}} \simeq 0.398$. The other quantity is the second moment of the distribution, $\langle s^2 \rangle_\lambda$,

$$\langle s^2 \rangle_\lambda = \int_0^\infty ds P_\lambda(s) s^2, \quad (3.6)$$

which takes the values $\langle s^2 \rangle_{\text{RMT}} \simeq \frac{3\pi}{8}$ and $\langle s^2 \rangle_{\text{Poisson}} = 2$ for the two types of statistics.

In the thermodynamic limit, the spectral density and the local average level spacing $\langle \Delta \lambda \rangle_\lambda \equiv \langle \lambda_{i+1} - \lambda_i \rangle_\lambda$ are related as $\rho(\lambda) \langle \Delta \lambda \rangle_\lambda = 1$. The same relation holds for the unfolded spectrum, and so, since the unfolded spectral density equals 1, one has $\langle s \rangle_\lambda \equiv \langle \Delta x \rangle_\lambda = 1$ in infinite volume. This might however fail in a finite volume, where the local averaging is necessarily done in a small but finite spectral interval,⁹ in regions where the spectral density is small and rapidly varying. Indeed, it is easy to see that the average level spacing in an interval of size Δ is given by the difference between the smallest eigenvalue λ' right above the end of the interval and the smallest eigenvalue λ inside the interval, divided by the number N of eigenvalues inside the interval. The spectral density associated to the given interval is

⁹In this case, when computing the average of $\lambda_{i+1} - \lambda_i$ we ask that λ_i be inside the interval, while λ_{i+1} can be outside.

simply N/Δ . If the spectral density is increasing, then one typically finds $\lambda' - \lambda < \Delta$, since eigenvalues get closer going up in the spectrum, and so $(N/\Delta) \cdot [(\lambda' - \lambda)/N] < 1$, from which we are led to expect $\rho(\lambda)\langle\Delta\lambda\rangle_\lambda < 1$, and so $\langle s \rangle_\lambda < 1$. This is what happens near the origin in the high temperature phase, where $\rho(\lambda) \sim \lambda^\alpha$ for some positive power α : the small spectral density requires the use of relatively large intervals over which the spectral density increases non-negligibly. The value of $\langle s \rangle_\lambda$ can then be used to assess the reliability of estimates of spectral statistics based on unfolding, and only those spectral regions where $\langle s \rangle_\lambda \simeq 1$ should be considered in further analyses.

From the point of view of the Dirac-Anderson approach, the model at hand should behave like a two-dimensional unitary Anderson model with on-site (diagonal) disorder.¹⁰ This model has been studied in Ref. [30], where it was shown that it displays an Anderson transition of Berezinskii-Kosterlitz-Thouless (BKT) type [55–57], with an exponentially divergent localisation length. We expect to find the same behaviour in our model in the high- β phase, with a mobility edge λ_c separating localised (low) and delocalised (high) Dirac modes, where the localisation length should diverge in the infinite-volume limit as

$$\xi \sim \exp \left\{ \frac{\alpha}{\sqrt{\lambda_c - \lambda}} \right\}, \quad (3.7)$$

for some constant α , as one approaches λ_c from the localised side, $\lambda < \lambda_c$. Points on the delocalised side, $\lambda > \lambda_c$, are all critical in a disorder-driven BKT transition, and so there the statistical properties of the spectrum should be independent of the volume (see Ref. [58]). To verify if this is the case, I did a finite-size scaling analysis of the spectral observables $\mathcal{O}_\lambda = I_\lambda, \langle s^2 \rangle_\lambda$, making the scaling hypothesis

$$\mathcal{O}_\lambda(L) = F \left((\lambda - \lambda_c)(\log L)^{\frac{1}{\nu}} \right), \quad (3.8)$$

with F some analytic function and L the linear size of the system. The one-parameter scaling hypothesis for localisation [59] is usually motivated by assuming that the behaviour of the system near the transition in a finite volume is determined only by the ratio $\xi(\lambda)/L$. However, since we are working on a lattice, ξ and L can be made dimensionless dividing them by the lattice spacing, and so one can use instead a function $F(r)$ of ratios of the more general form $r = h(\xi(\lambda))/h(L)$. Indeed, since near the transition and for large volumes only the leading behaviour of h matters, r is invariant under the rescaling $\xi \rightarrow b\xi$, $L \rightarrow bL$, as it should. On the other hand, analyticity in a finite volume constrains the form of h , which in the case at hand must be of the form $h(\xi) = 1/(\log \xi)^{\frac{1}{\nu}}$, where $\nu = \frac{1}{2}$ if Eq. (3.7) holds.

4 Numerical results

In this Section I report on the results of a numerical investigation of Dirac spectra in finite-temperature SU(3) pure-gauge theory in 2+1 dimensions on the lattice. The gauge back-

¹⁰Off-diagonal disorder is present as well, but does not play an important role in localising the eigenmodes [53, 54].

N_s	n° of eigenvalues	n° of configurations
32	100	40000
40	140	40000
48	216	20000
56	280	8000
64	380	4000
72	480	2000

Table 1. Number of eigenvalues and sample size for the various volumes.

grounds were obtained via Monte Carlo simulations of the partition function Eq. (3.3), using a hypercubic lattice of fixed temporal extension $N_t = 4$ and spatial extension $N_s = 32, 40, 48, 56, 64, 72$ in lattice units, for several values of $\bar{\beta}$, both in the confined and the deconfined phases. Right above the deconfinement transition, and for the lattice sizes used here, a system initialised in the trivial Polyakov-loop sector is still able to switch to one of the complex sectors, and to temporarily tunnel to the confined phase, even though this becomes less and less likely as the volume is increased. For $\bar{\beta} = 5.05, 5.10, 5.15, 5.20$ I then always analysed the gauge configuration obtained by rotating the centre sector to the trivial one, as explained above in Section 3. For $\bar{\beta} = 5.25, 5.50, 5.75, 6.00, 6.25, 6.50$ this was not necessary, as a system initialised in the trivial Polyakov-loop sector never left it. Of course, no sector switching was used for $\bar{\beta} = 2.50, 3.00, 4.00$ in the confined phase. The first few eigenvalues of the staggered Dirac operator were obtained by means of the ARPACK routine [60]. In the following I denote with λ the (imaginary part of the) eigenvalues of the staggered Dirac operator in lattice units. Monte Carlo simulations were performed with standard heatbath [61, 62] and overrelaxation [63, 64] algorithms. Details about statistics and the number of computed eigenvalues for each volume can be found in Table 1. All statistical errors were obtained through a jackknife analysis with 100 samples. All fits in this work were done using the MINUIT routine [65], establishing the accuracy of the errors with the MINOS subroutine. Whenever the difference is negligible, the symmetric parabolic error is used instead.

4.1 Participation ratio

I discuss first the PR of the low modes. In Fig. 1 I show how the average PR of the Dirac modes computed locally in the spectrum, $\langle \text{PR} \rangle_\lambda$, changes along the spectrum for $\bar{\beta} = 5.50$ (in the deconfined phase) and the various lattice volumes. All locally averaged quantities, like $\langle \text{PR} \rangle_\lambda$, are obtained by averaging the relevant observable over the modes in spectral intervals of size $w = 0.005$ and over gauge configurations; the result is assigned to the average eigenvalue (computed similarly) in that interval. In the top panel of Fig. 1 I show $\langle \text{PR} \rangle_\lambda$: it is clear that this quantity keeps decreasing with the volume for the lowest modes, while it remains almost constant for the higher modes. In the bottom panel I show instead $\langle \text{PR} \rangle_\lambda \cdot V$, i.e., the spatial “size” of the mode in lattice units: this remains constant for the lowest modes, and blows up for the higher modes. This shows that the lowest modes are localised, and the

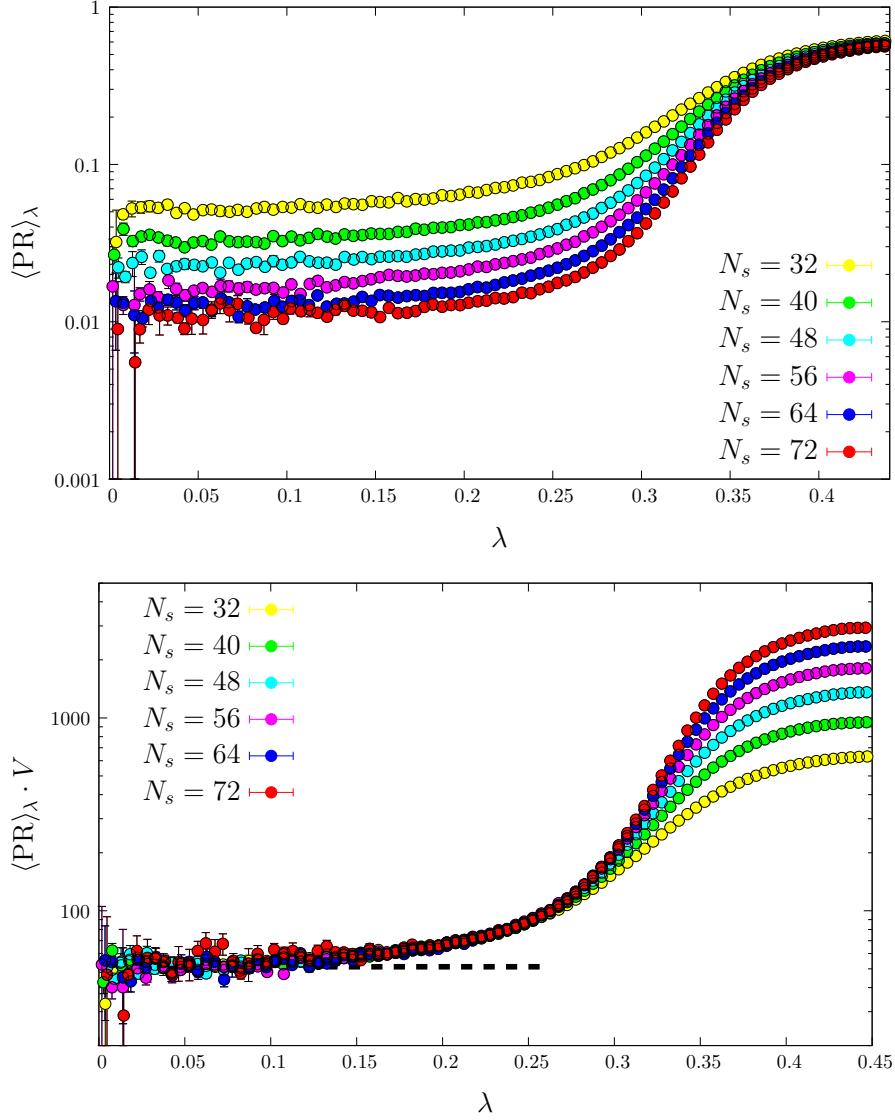


Figure 1. Participation ratio $\langle \text{PR} \rangle_\lambda$ (top), and size $\langle \text{PR} \rangle_\lambda \cdot V$ (bottom) of Dirac eigenmodes at $\bar{\beta} = 5.50$ as a function of the spectral region for various volumes (in logarithmic scale). The dashed line in the bottom panel is the PR of the lowest mode extrapolated to infinite lattice size (see text).

higher ones are delocalised. Furthermore, the size of the modes is approximately constant in the localised part of the spectrum. A similar behaviour is observed at all $\bar{\beta}$ in the deconfined phase. For the lowest two values of $\bar{\beta}$ there, i.e., $\bar{\beta} = 5.05, 5.10$, the volume dependence appears to be non-monotonic. This is probably caused by large finite-size effects near the critical temperature (see below).

To give a well-defined estimate of the size of a localised mode in the deconfined phase, I have measured the PR of the lowest mode averaged over configurations times the spatial size of the lattice, $\langle \text{PR}_1 \rangle \cdot V$, and extrapolated it to infinite volume. Data points lie approximately

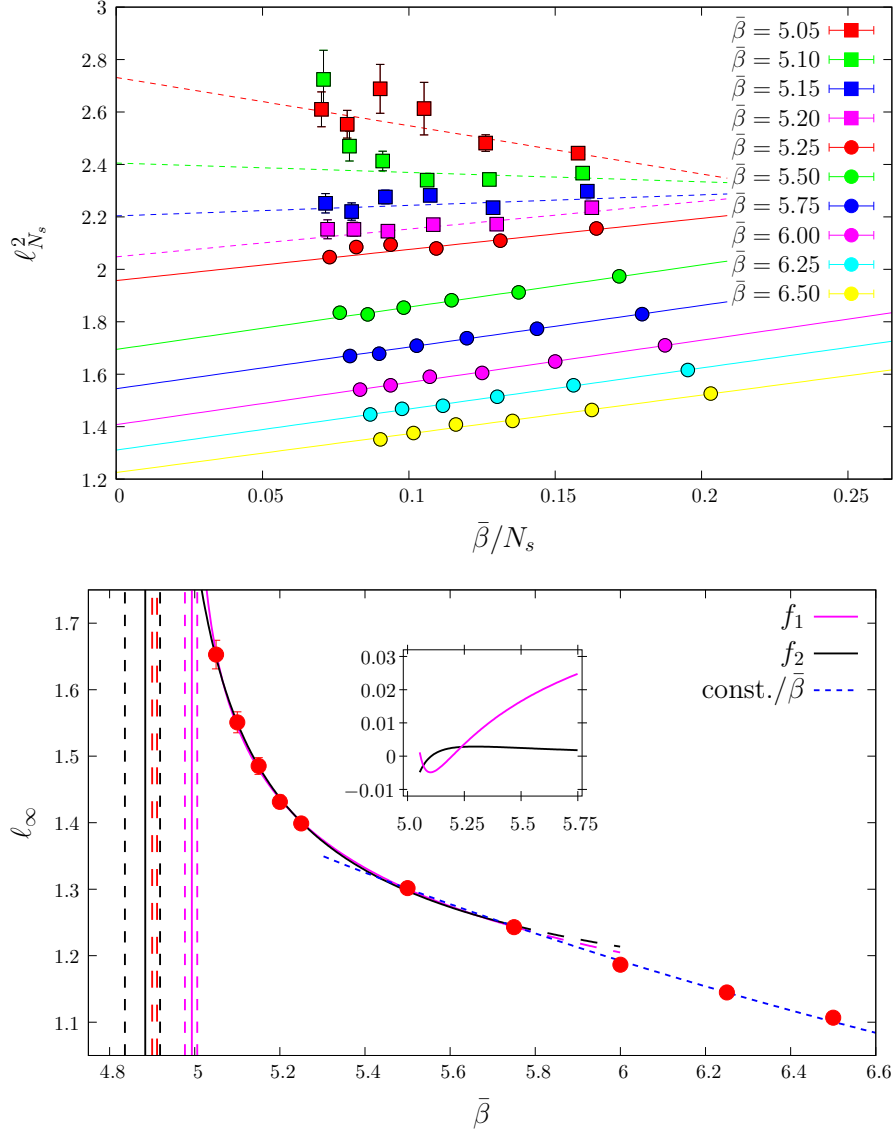


Figure 2. Top panel: size $\ell_{N_s}^2$ of the lowest mode in physical units as a function of the inverse linear size of the lattice, for various $\bar{\beta}$ in the deconfined phase. Linear fits are also shown with solid lines. Bottom panel: linear size ℓ_∞ extrapolated to infinite volume as a function of $\bar{\beta}$. Fits to the near- $\bar{\beta}_c$ data with the functions $f_1(\bar{\beta})$ (magenta) and $f_2(\bar{\beta})$ (black) given in Eq. (4.2) are also shown. The corresponding fitted values for $\bar{\beta}_{1,2}$ and the related error bands are marked by the vertical lines with corresponding colours. The error band for $\bar{\beta}_c$ is also shown (red). In the inset it is shown the change in the fitting function due to changing the fitting interval (see text).

on straight lines when plotted against the inverse linear size of the lattice [see Fig. 2 (top)], so a linear extrapolation in $1/N_s$ seemed appropriate. The results compare well with the approximate plateau of $\langle \text{PR} \rangle_\lambda \cdot V$, see the dashed line in Fig. 1 (bottom). Not surprisingly, this is less so for the lowest two values of $\bar{\beta}$. In Fig. 2 (top) I show the size $\ell_{N_s}^2$ of the lowest

parameter	$i = 1$	$i = 2$
a_i	$1.2058^{+0.0040}_{-0.0039}$	$0.2045^{+0.0037}_{-0.0029}$
$\bar{\beta}_i$	$4.993^{+0.012}_{-0.016}$	$4.884^{+0.035}_{-0.048}$
c_i	$0.1107^{+0.0077}_{-0.0066}$	$0.498^{+0.061}_{-0.048}$

Table 2. Results of fits to ℓ_∞ with the functional forms $f_i(\bar{\beta})$ of Eq. (4.2).

mode in physical units¹¹ for the various volumes and values of $\bar{\beta}$,

$$\ell_{N_s}^2 \equiv \langle \text{PR}_1 \rangle \left(\frac{N_s}{\bar{\beta}} \right)^2. \quad (4.1)$$

The linear extrapolation in $\bar{\beta}/N_s$ is fully satisfactory for all values of $\bar{\beta}$, except for the lowest two, for which the linear fit to the data is of poorer quality. Nonetheless, the result of the extrapolation is in agreement with the general trend of the data, which shows the size of the lowest mode increasing as one gets closer to the critical coupling. If, as expected, all the modes become delocalised at the deconfinement point, then this quantity should blow up there. Near the critical point, the size of the lowest mode in lattice units, $\ell_\infty \bar{\beta}$, can then become comparable to N_s for the available lattice sizes, causing sizeable finite-size effects. The results for $\ell_\infty \bar{\beta}$ vary from around 7 for the highest values of $\bar{\beta}$, to around 8 for the ones closest to $\bar{\beta}_c$, so there is probably nothing to worry about for the lattice sizes used in this work. On the other hand, if localisation is driven by the behaviour of the Polyakov line, then near the critical point one expects further large finite-size effects due to the large fluctuations of this quantity (see also the discussion below in Section 4.2). In particular, during the numerical simulations the system can still tunnel between the confined and deconfined phases for not large enough volumes. Although these effects are harder to quantify, they are probably responsible for the larger error bars of ℓ_{N_s} near $\bar{\beta}_c$.

The results of the infinite-volume extrapolation of ℓ_{N_s} are shown in Fig. 2 (bottom). For the lowest values of $\bar{\beta}$, even though one may not fully trust quantitatively the results due to the above-mentioned finite-size effects, there is a clear sign of a divergence as the critical coupling is approached. At large $\bar{\beta}$ instead this quantity decreases as $1/\bar{\beta}$, reflecting the fact that there the extrapolated size of the lowest mode in lattice units is almost independent of the coupling. A constant fit using only $\bar{\beta} \geq 5.50$ yields $\ell_\infty \bar{\beta} = 7.155(10)$ with $\chi^2/\text{d.o.f.} = 1.4$. This leads to a linear dependence of the physical linear size of the mode on the inverse temperature at high temperature, as one would expect given that this is the most important scale there. The same behaviour has been observed in QCD [16]. Plugging in the fit result, one gets $\ell_\infty T = 1.7887(25)$, where $T \equiv \bar{\beta}/N_t$. Despite the limited number of points close to $\bar{\beta}_c$, I have tried to fit the divergent behaviour with the following functional forms,

$$f_1(\bar{\beta}) = \frac{a_1}{(\bar{\beta} - \bar{\beta}_1)^{c_1}}, \quad f_2(\bar{\beta}) = \exp \left\{ \frac{a_2}{(\bar{\beta} - \bar{\beta}_2)^{c_2}} \right\}. \quad (4.2)$$

¹¹I use a system of “natural” units in which $g^2/2 = 1$, so that the lattice spacing is dimensionless.

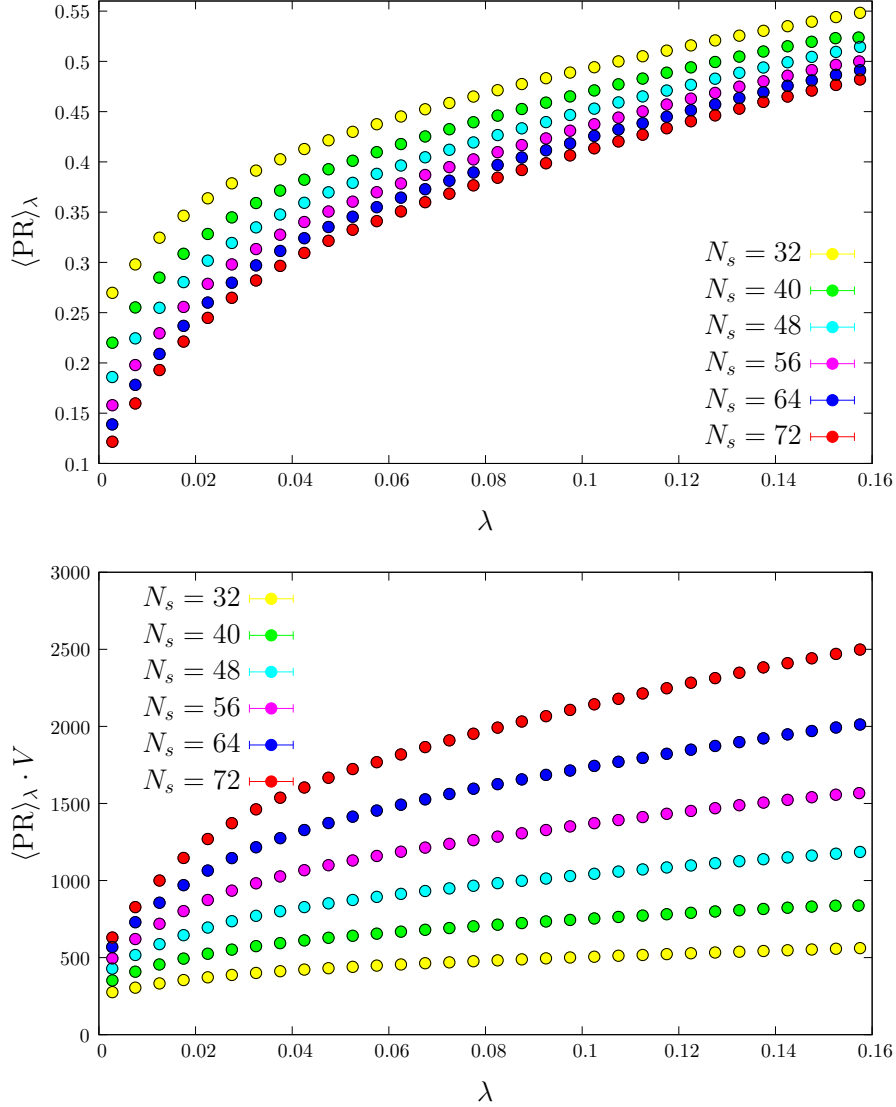


Figure 3. Participation ratio $\langle \text{PR} \rangle_\lambda$ (top), and size $\langle \text{PR} \rangle_\lambda \cdot V$ (bottom) of Dirac eigenmodes at $\bar{\beta} = 3.00$ as a function of the spectral region for various volumes.

The first one is a simple power-law, while the second one is inspired by the behaviour of the localisation length¹² at criticality.¹³ Only points up to $\bar{\beta} = 5.75$ were included. Both fits converge, with suspiciously small $\chi^2/\text{d.o.f.} \simeq 0.2$ and $\chi^2/\text{d.o.f.} \simeq 0.5$, respectively, indicating

¹²It must be remarked that in general the localisation length, ξ , and the quantities $\ell^{(q)} = (\text{IPR}_q)^{-\frac{1}{2(q-1)}}$ built out of the generalised IPRs (see footnote 5), do not have the same critical behaviour. In fact, even though all these quantities provide an estimate of the size of the localised modes and should blow up at the critical point, they are sensitive to different features of the modes, which usually results in different critical exponents.

¹³The critical behaviour of ξ should not depend on whether the critical line is crossed in the direction of the eigenvalues at fixed $\bar{\beta}$, or in the direction of $\bar{\beta}$ at fixed eigenvalue. Having extrapolated the lowest mode to infinite volume, here we are looking at around $\lambda = 0$.

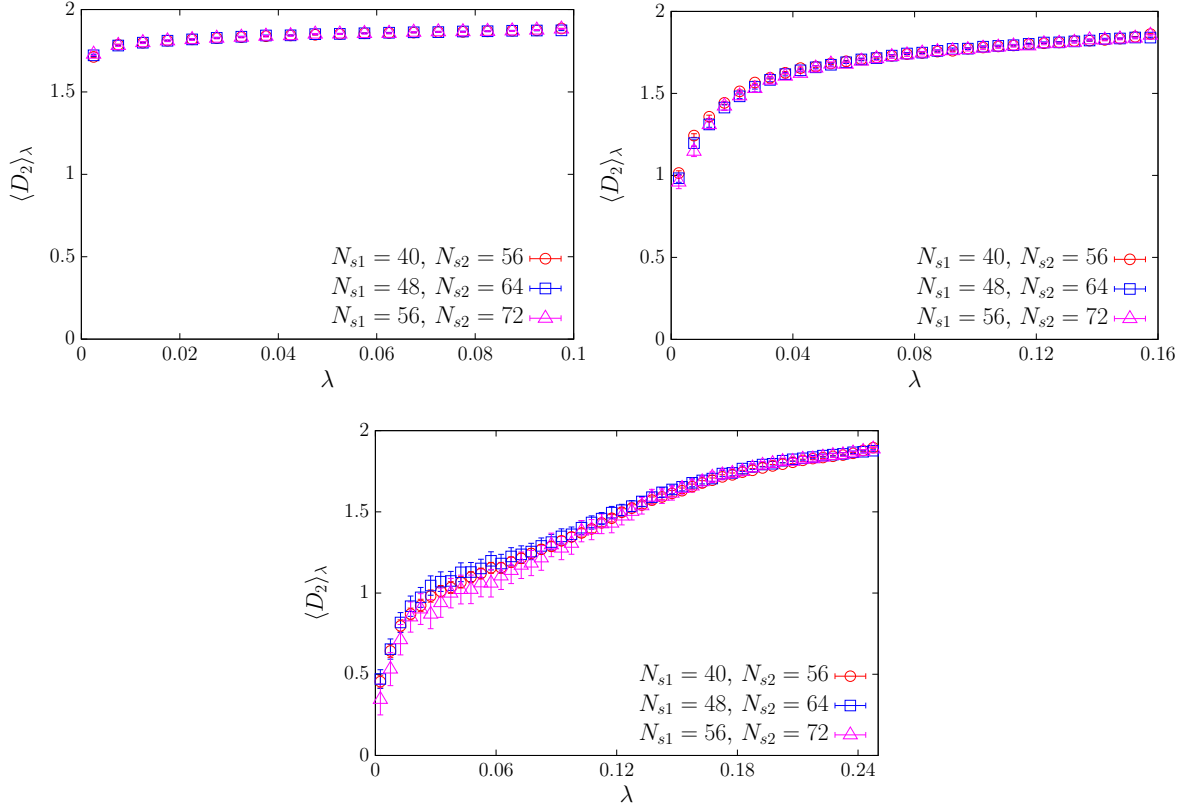


Figure 4. Fractal dimension of the Dirac eigenmodes as a function of the spectral region in the confined phase, for $\bar{\beta} = 2.50$ (top left), $\bar{\beta} = 3.00$ (top right), and $\bar{\beta} = 4.00$ (bottom).

a fair amount of overfitting. The values obtained for the delocalisation point, $\bar{\beta}_{1,2}$, are reported in Table 2. While $\bar{\beta}_1$ is inconsistent with the critical lattice coupling $\bar{\beta}_c = 4.9057(57)$ [49], $\bar{\beta}_2$ is in fair agreement with it. To check which functional form describes better the data, I restricted the fit to points up to $\bar{\beta} = 5.25$ only. Again both fits converge, with an even bigger amount of overfitting ($\chi^2/\text{d.o.f.} \simeq 0.1$ and $\chi^2/\text{d.o.f.} \simeq 0.08$, respectively), and increased statistical errors on the parameters. The important point, however, is that while f_1 changes visibly in the region left out of the fit (up to 2%), f_2 changes very little (always less than 0.2%). I take this as an indication that f_2 captures better the singular behaviour of ℓ_∞ . Despite all the limitations of the present analysis, one can quite safely conclude that the results are compatible with localised modes appearing at $\bar{\beta}_c$ in the thermodynamic limit. Quite interestingly, the result for the critical exponent c_2 found using $f_2(\bar{\beta})$ is surprisingly close to the critical exponent of the localisation length $\nu = \frac{1}{2}$. Even though no firm conclusion can be reached yet based on this result, it suggests nonetheless the possibility that the generalised IPRs (see footnote 5) may vanish exponentially rather than as power laws as the critical point is approached.

The behaviour of the PR in the confined phase is different, although apparently still

nontrivial. In Fig. 3 I show $\langle \text{PR} \rangle_\lambda$ and $\langle \text{PR} \rangle_\lambda \cdot V$ for $\bar{\beta} = 3.00$ for the various lattice sizes. None of these two quantities shows a clear sign of converging to a constant anywhere in the available spectrum, indicating that they show a somewhat intermediate behaviour between localised and fully delocalised. To investigate this issue quantitatively, one can compute the fractal dimension D_2 , related to the PR as [21]

$$\text{PR} \sim L^{D_2-d} = L^{D_2-2}, \quad (4.3)$$

where \sim denotes the asymptotic large-volume behaviour and L is the linear size of the system. For fully delocalised modes $D_2 = 2$, while for localised modes $D_2 = 0$. The fractal dimension D_2 can be estimated by comparing the PR computed on pairs of lattices of linear spatial sizes N_{s1} and N_{s2} , using the formula

$$D_2(N_{s1}, N_{s2}) = 2 + \frac{\log(\text{PR}(N_{s1})/\text{PR}(N_{s2}))}{\log(N_{s1}/N_{s2})}. \quad (4.4)$$

From this estimator one obtains D_2 in the limit of large $N_{s1,2}$. The results for $\bar{\beta} = 2.50, 3.00, 4.00$ are shown in Fig. 4 for three different pairs of volumes. The volume dependence is mild to non-existent. Low modes have a nontrivial fractal dimension between 0 and 2, while for higher modes D_2 approaches 2. Moreover, low modes are closer and closer to being localised as one approaches the critical temperature from below.

4.2 Spectral statistics

As mentioned above in Section 2, spectral statistics can be used to study the localisation properties of the Dirac modes and to determine efficiently the mobility edge and the related critical properties. The typical behaviour of I_λ and $\langle s^2 \rangle_\lambda$ in the deconfined phase is shown in Fig. 5 for $\bar{\beta} = 6.25$. Low modes are close to having Poisson statistics, and more and more so as the size of the lattice increases. For every lattice size the statistics change from Poisson to RMT-type, more precisely to GUE-type, as one moves up along the spectrum. At some point the curves corresponding to the various volumes merge, and show little to no dependence on the volume. This is precisely the behaviour expected for a disorder-driven BKT transition in the spectrum. To make this statement quantitative, I verified the scaling hypothesis Eq. (3.8) by fitting the data for I_λ for various volumes with the rational function

$$F(\lambda, N_s) = \frac{c_1 + c_2 y(\lambda, N_s) + c_3 y(\lambda, N_s)^2 + c_4 y(\lambda, N_s)^3}{1 + \bar{c}_1 y(\lambda, N_s) + \bar{c}_2 y(\lambda, N_s)^2}, \quad (4.5)$$

$$y(\lambda, N_s) = (\lambda - \lambda_c)(\log N_s)^{\frac{1}{\nu}}.$$

The fit was performed restricting to an interval of width $w = 0.06$ centred at the merging point of the curves, and including volumes with $N_s \geq N_{s \min}$ for $N_{s \min} = 32, 40, 48$. I obtained reasonable values of $\chi^2/\text{d.o.f.}$, ranging between 1 and 2.15 for $N_{s \min} = 32$, between 0.5 and 1.05 for $N_{s \min} = 40$, and between 0.35 and 0.65 for $N_{s \min} = 48$. The results for the critical exponent ν , shown in Fig. 6, are in fair agreement with the theoretically expected value $\nu = \frac{1}{2}$.

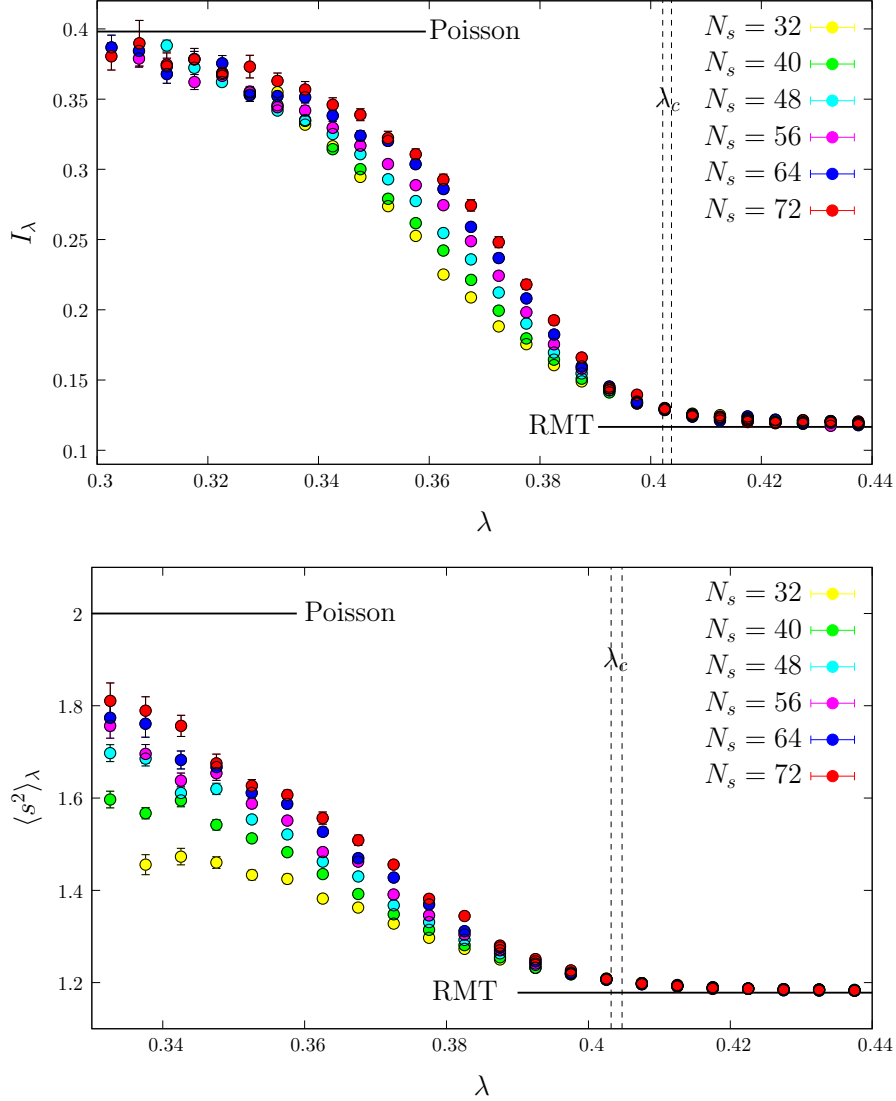


Figure 5. Dependence on the spectral region for I_λ (top) and $\langle s^2 \rangle_\lambda$ (bottom) in the deconfined phase at $\bar{\beta} = 6.25$ for several volumes. Only points with $\langle s \rangle_\lambda$ close to 1 are shown. The position of the mobility edge and its uncertainty, as determined via a finite-size scaling analysis, are also shown.

Fits to the data with Eq. (4.5) are quite sensitive to the initial values of the fitting parameters and the choice of fitting interval, and sometimes the error estimate of the parameters provided by MINOS is not accurate, especially close to the critical coupling (the missing point at $\bar{\beta} = 5.15$ for $N_{s\min} = 48$ in Fig. 6 is precisely a case of inaccurate error estimate). Despite these numerical shortcomings, the results are all quite consistent with the hypothesis $\nu = \frac{1}{2}$. In fact, I performed these fits to obtain an unbiased (or at least as little biased as possible) estimate of the critical exponent, as a preliminary step for a more accurate and more systematic finite-size scaling study using constrained fits [66]. These fits turn out to

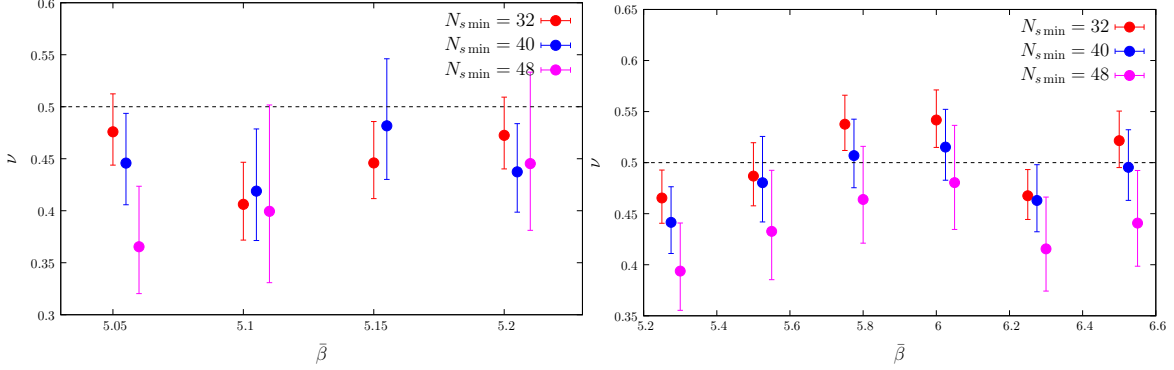


Figure 6. Critical exponent ν obtained via an unconstrained fit with the function Eq. (4.5) to the data for the spectral statistic I_λ in the deconfined phase, close to the transition (left panel) and farther above the transition (right panel).

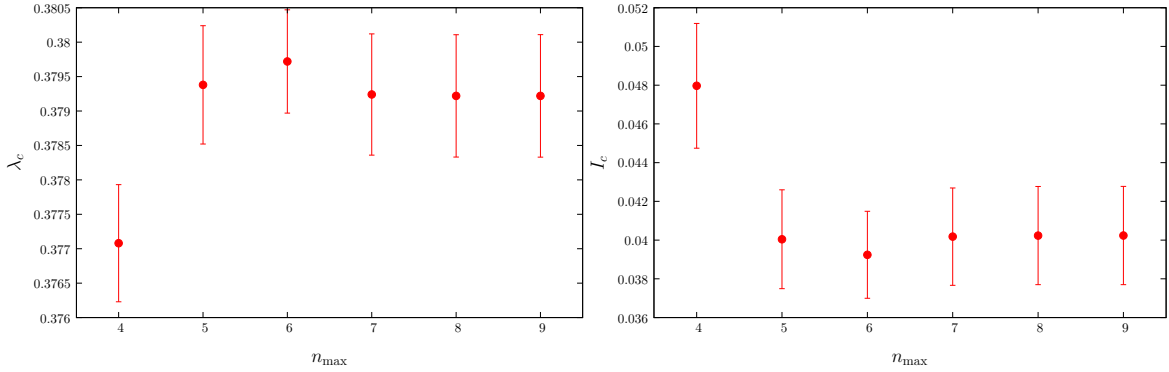


Figure 7. Dependence of the fitted values of λ_c (left) and I_c (right) on the order of the polynomial in a constrained fit to the data for the spectral statistic I_λ obtained at $\bar{\beta} = 5.75$, using $w = 0.06$, $N_{s \min} = 40$ and $\sigma = 8$.

be unstable if ν is not constrained strongly, for which reason I preferred to first check the viability of the theoretical value with unconstrained fits, and then perform the constrained fits fixing $\nu = \frac{1}{2}$. Constrained fits were done by fitting the data with polynomial functions,

$$F(\lambda, N_s) = \sum_{n=0}^{n_{\max}} F_n y(\lambda, N_s)^n, \quad (4.6)$$

where $y(\lambda, N_s)$ is given in Eq. (4.5), which is nothing but a truncated Taylor expansion around λ_c . The coefficients F_n and the mobility edge λ_c are the fitting parameters. In general, in a constrained fit one minimises an augmented χ^2 , $\chi_{\text{aug}}^2 = \chi^2 + \chi_{\text{prior}}^2$, where

$$\chi_{\text{prior}}^2 = \frac{(\lambda_c - \lambda_c^{(0)})^2}{\sigma_{\lambda_c}^2} + \frac{(\nu - \nu^{(0)})^2}{\sigma_\nu^2} + \sum_{n=0}^{n_{\max}} \frac{(F_n - F_n^{(0)})^2}{\sigma_n^2}, \quad (4.7)$$

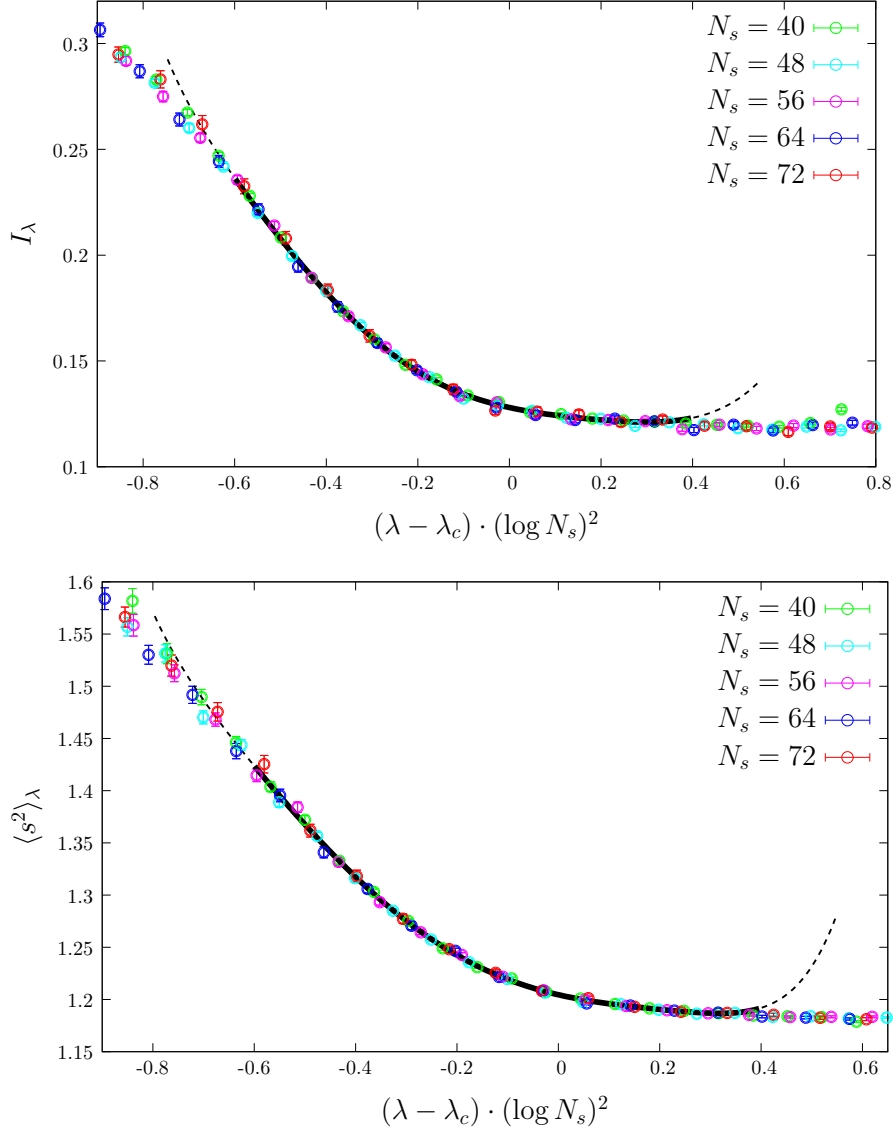


Figure 8. Scaling behaviour of I_λ (top) and $\langle s^2 \rangle_\lambda$ (bottom) at $\bar{\beta} = 5.75$. The scaling function (solid line) was obtained via constrained fitting using $w = 0.06$, $N_{s \min} = 40$ and $\sigma = 8$. The scaling behaviour is seen to persist also outside the range where the fit was performed, where the fitted function does not match the data points (dashed line).

with properly chosen priors $\lambda_c^{(0)}$, $\nu^{(0)}$, $F_n^{(0)}$ and σ_{λ_c} , σ_ν , σ_n , reflecting one's knowledge of the parameters. The order n_{\max} of the polynomial is then increased until the error on the parameters stabilises. This allows to estimate accurately the systematic error due to truncation [66]. In my analysis I used no prior for the first four coefficients and for the mobility edge (so formally setting $\sigma_{\lambda_c} = \sigma_1 = \sigma_2 = \sigma_3 = \sigma_4 = \infty$), I fixed $\nu = \frac{1}{2}$ (so formally setting $\sigma_\nu = 0$), and set $F_n^{(0)} = 0$ and a rather loose and constant width $\sigma_n = \sigma$ for $n \geq 5$. I repeated the analysis

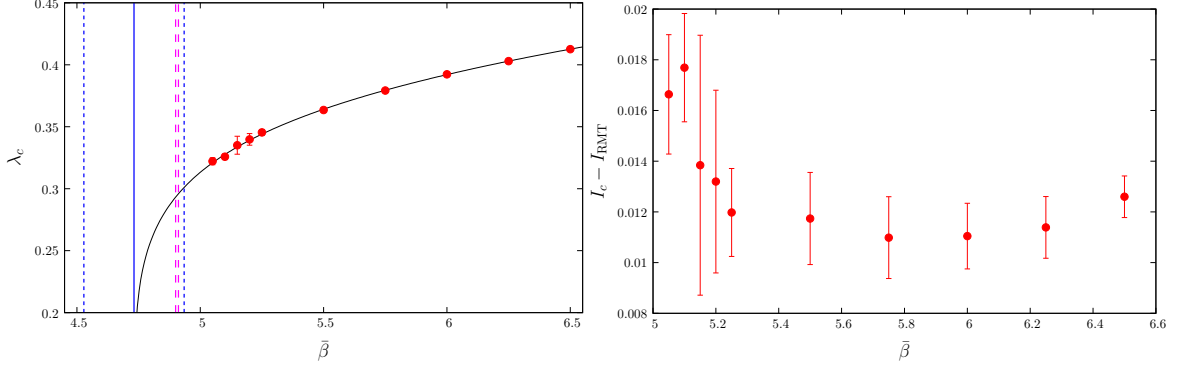


Figure 9. Mobility edge λ_c (in lattice units) obtained via constrained fitting using I_λ (left), and deviation of the corresponding value I_c of the statistic at the critical point from the RMT value (right). The result of a fit of λ_c with Eq. (4.8) is also shown (solid line), together with the value $\bar{\beta}_0$ at which the mobility edge extrapolates to zero and corresponding error band (blue lines), and with the error band for the critical lattice coupling for deconfinement obtained in Ref. [49] (magenta lines).

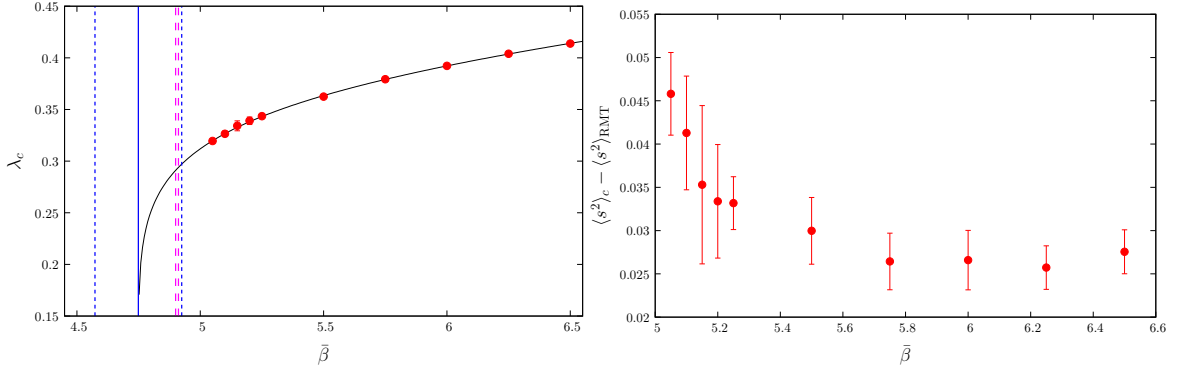


Figure 10. Mobility edge λ_c (in lattice units) obtained via constrained fitting using $\langle s^2 \rangle_\lambda$ (left), and deviation of the corresponding value $\langle s^2 \rangle_c$ of the statistic at the critical point from the RMT value (right). The result of a fit of λ_c with Eq. (4.8) is also shown (solid line), together with the value $\bar{\beta}_0$ at which the mobility edge extrapolates to zero and corresponding error band (blue lines), and with the error band for the critical lattice coupling for deconfinement obtained in Ref. [49] (magenta lines).

for $\sigma = 3, 5, 8$, with little variation of the results. I used spectral intervals of width $w = 0.055$ and $w = 0.06$ around the merging point of the curves, and included data for $N_s \geq N_{s\min}$ with $N_{s\min} = 40, 48$. This was done to check further sources of systematic error. The order n_{\max} of the polynomial was increased up to $n_{\max} = 9$. The typical results of the constrained fitting procedure are shown in Fig. 7, where I show λ_c and the value $I_c \equiv I_{\lambda_c} = F_0$ of I_λ at the mobility edge, obtained by fitting I_λ for $\bar{\beta} = 5.75$, $w = 0.06$, $N_{s\min} = 40$ and $\sigma = 8$. The convergence of the central values and of the errors is clear. The procedure was then repeated for the spectral statistic $\langle s^2 \rangle_\lambda$. The quality of the scaling can be seen in Fig. 8.

The final results were obtained by collecting all the central values obtained with the choice $(w, N_{s\min}, \sigma) = (0.06, 40, 8)$. The final error was obtained by adding in quadrature

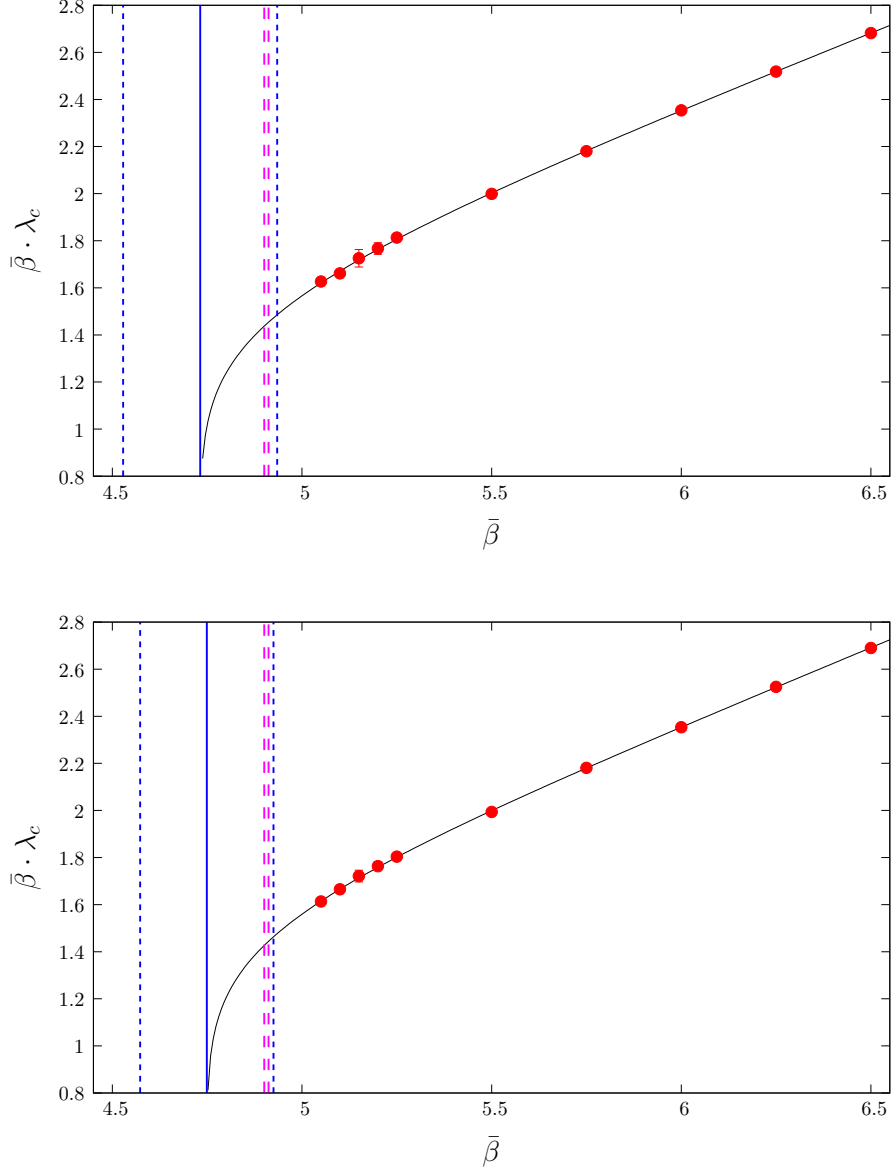


Figure 11. Mobility edge $\lambda_{c\text{phys}} = \bar{\beta} \cdot \lambda_c$ in physical units, as obtained fitting I_λ (top) and $\langle s^2 \rangle_\lambda$ (bottom). The function $\bar{\beta}h(\bar{\beta})$ [see Eq. (4.8)] obtained fitting λ_c is also shown (solid line). The positions of $\bar{\beta}_0$ and corresponding error band (blue line) and the error band of $\bar{\beta}_c$ (magenta line) are also shown.

the statistical error (as estimated by MINUIT¹⁴) and the three systematic errors, namely those related to the width of the prior distribution, width of the fitting interval, and minimal lattice size. In turn, these were estimated as the absolute value of the difference between the final results and the central values obtained with $(w, N_{s\text{min}}, \sigma) = (0.06, 40, 5)$, $(0.055, 40, 8)$,

¹⁴The symmetric parabolic error was used, since it never differed from the MINOS errors by more than 10%.

and (0.06, 48, 8), respectively. Among the various fitting parameters, the most important ones are the mobility edge, λ_c , and the values of the statistics at the critical point, $I_c \equiv I_{\lambda_c}$ and $\langle s^2 \rangle_c \equiv \langle s^2 \rangle_{\lambda_c}$. These are shown in Figs. 9 and 10. The mobility edge in physical units, $\lambda_{c\text{phys}}(\beta) = \beta\lambda_c(\beta)$, obtained multiplying λ_c by the lattice coupling (assuming perfect scaling) is shown in Fig. 11. The values of $\lambda_c(\bar{\beta})$ obtained from the two spectral statistics agree with each other within errors. The values of the spectral statistics at the mobility edge differ from those corresponding to Poisson or RMT statistics, and depend on the lattice coupling (see Figs. 9 and 10). As functions of $\bar{\beta}$ they are rather flat at large $\bar{\beta}$, while they seem to grow as one approaches the critical temperature. This is different from what has been observed in QCD and QCD-like models in 3+1 dimensions: there the statistics at the mobility edge have always been found to be compatible with the critical statistics of the three-dimensional unitary Anderson model [23, 67].

Finally, I fitted the mobility edge in lattice units, $\lambda_c(\bar{\beta})$, as obtained from the two spectral statistics, as a function of $\bar{\beta}$, trying to establish if it extrapolates to zero at a coupling compatible with the critical one. In order to estimate accurately the errors, I performed another constrained fit with a function of the form

$$h(\bar{\beta}) = u(\bar{\beta} - \bar{\beta}_0)^v \left(1 + \sum_{m=1}^{m_{\max}} h_m(\bar{\beta} - \bar{\beta}_0)^m \right), \quad (4.8)$$

increasing m_{\max} up to $m_{\max} = 5$. While no prior was assumed on u , v and $\bar{\beta}_0$, the parameters h_m were constrained to be small, centring their distributions at zero and using widths $\sigma_1 = \sigma_2 = 0.05$, $\sigma_3 = 0.005$, $\sigma_4 = 0.001$, and $\sigma_5 = 0.0005$. These values were chosen so that the fit would converge and errors would be estimated accurately by MINOS. While the resulting errors on h_m are bigger than the central values, so that these coefficients are compatible with zero, nevertheless their presence in the fit has a visible impact on the errors of the important parameters. This can be seen in Fig. 12, where I show the dependence on m_{\max} of $\bar{\beta}_0$ and its error. The final results for u , v and $\bar{\beta}_0$, determined from both the I_λ and the $\langle s^2 \rangle_\lambda$ analyses, are reported in Table 3. The $\chi_{\text{aug}}^2/n_{\text{data}}$ is around 0.2 in both cases, a suspiciously small value that can however be explained as follows.¹⁵ In Figs. 9 and 10 one sees that the data points at $\bar{\beta} = 5.15, 5.20$ have a considerably larger error than the other points. This is due to a rather large finite-volume effect: values of λ_c determined with $N_{s\text{min}} = 48$ show a visible jump upwards with respect to those determined with $N_{s\text{min}} = 40$, something that does not happen for the other values of $\bar{\beta}$. This suggests that it is probably due to a fit instability that would be cured by increasing the statistics, and thus that the finite-volume error is actually overestimated. The results obtained at $\bar{\beta} = 5.15, 5.20$ with $N_{s\text{min}} = 40$ are probably more reliable than those obtained with $N_{s\text{min}} = 48$, and so data with $N_{s\text{min}} = 40$ have been used as central values. Repeating the fit with Eq. (4.8) using these data and only the statistical errors leads to similar results with a $\chi_{\text{aug}}^2/n_{\text{data}}$ of about 0.7–0.8.

¹⁵It must be noted that for constrained fits the quantity to check is $\chi_{\text{aug}}^2/n_{\text{data}}$ with n_{data} the number of data points, and that while this quantity should be around 1, it is the convergence of the errors on the fit parameters that determines the quality of the fits [66].

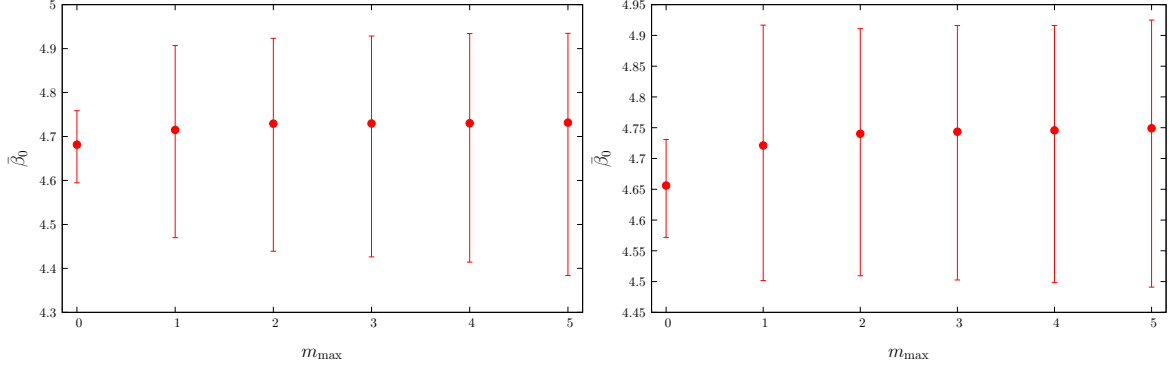


Figure 12. Dependence of $\bar{\beta}_0$ and v on m_{\max} in a constrained fit of $\lambda_c(\bar{\beta})$, obtained from I_λ (left) and $\langle s^2 \rangle_\lambda$ (right), with the function Eq. (4.8).

parameter	from I_λ	from $\langle s^2 \rangle_\lambda$
u	$0.377^{+0.014}_{-0.017}$	$0.375^{+0.013}_{-0.012}$
v	$0.141^{+0.12}_{-0.053}$	$0.135^{+0.095}_{-0.049}$
$\bar{\beta}_0$	$4.73^{+0.15}_{-0.35}$	$4.75^{+0.13}_{-0.26}$

Table 3. Results for $\bar{\beta}_0$, u , and v obtained with a constrained fit of $\lambda_c(\bar{\beta})$, obtained from I_λ (left) and $\langle s^2 \rangle_\lambda$ (right), with the function Eq. (4.8), using $m_{\max} = 5$.

In Figs. 9 and 10 I also show the fit to the λ_c data with Eq. (4.8), marking the critical point $\bar{\beta}_0$ at which the mobility edge vanishes, and the corresponding error band. The critical coupling $\bar{\beta}_c$ for deconfinement, as determined in Ref. [49], is also shown. The two values agree within one standard deviation, although they just do so. We could just be happy with that and conclude that the mobility edge vanishes at the deconfinement transition, but it is worth trying to explain why the difference is sizeable. According to the sea/islands picture and the Dirac-Anderson approach, the source of disorder leading to localisation in the deconfined phase are the local fluctuations of the Polyakov lines around the ordered value. One then expects the mobility edge to be sensitive to the average Polyakov loop, since this provides a measure of how ordered the system is. Finite-size effects affecting this quantity should then reflect themselves both on the mobility edge and on the pseudocritical coupling in a finite volume. To try to quantify finite-size effects on the latter quantity, I used the results of Ref. [49]. There, the critical coupling in the infinite-volume limit for the 2+1 dimensional SU(3) pure gauge theory is obtained via extrapolation from finite volumes using the formula

$$\frac{\beta_c(\infty) - \beta_c(N_s)}{\beta_c(\infty)} = h \left(\frac{N_t}{N_s} \right)^{\frac{6}{5}}, \quad (4.9)$$

where $\beta_c(N_s)$ is the pseudocritical coupling defined as the position of the peak of the Polyakov loop susceptibility, h is a fitting parameter, and the exponent is the one appropriate for a second-order phase transition in the universality class of the two-dimensional $q = 3$ Potts model. Although not reported explicitly, the value of h for SU(3) can be estimated by

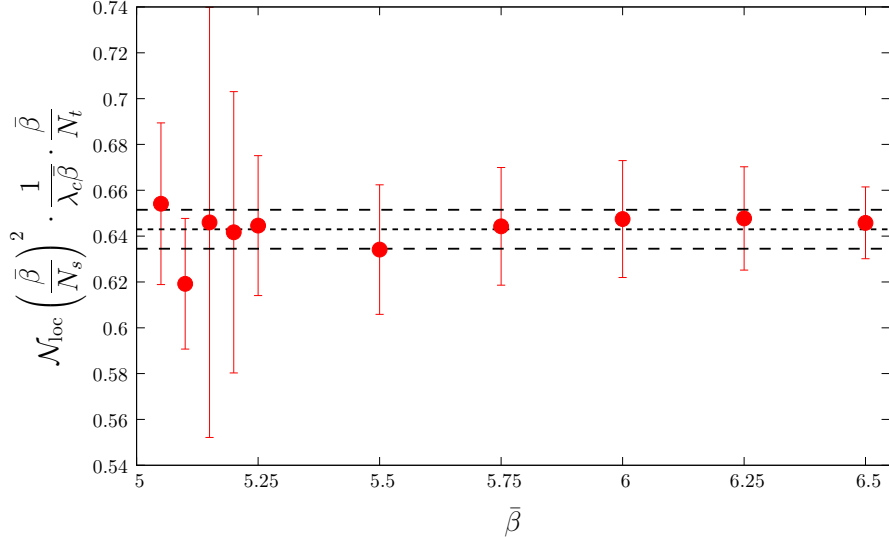


Figure 13. Density of localised modes times $T/\lambda_{c\text{phys}}$ in physical units. A constant fit and the corresponding error band (dashed lines) are also shown.

using the reported values for $SU(N_c)$ with $N_c = 4, 5, 6, 8$ and the approximate behaviour $h(N_c)N_c^2 \simeq a + b/N_c^2$. Using the $N_t = 4$ data, this yields $h(3) \simeq 1.2$, and in turn a finite-volume pseudocritical coupling $\bar{\beta}_c(72) \simeq 4.7$ for $N_s = 72$, corresponding to the largest volume used in this work. Although this value is remarkably close to the results for $\bar{\beta}_0$ in Table 3, it should not be taken too literally. The important point is that the deviation from the infinite-volume limit is still about 4% for $N_s = 72$, which is just about the same deviation we find between $\bar{\beta}_0$ and the infinite-volume result for $\bar{\beta}_c$. If anything, this is reinforcing rather than weakening the claim that deconfinement and localisation of the low modes happen together. In this respect, it might be worth mentioning that the exponent v in Table 3, governing the approach to zero of the mobility edge, agrees (within the rather large errors) with the magnetisation critical exponent governing the vanishing of the Polyakov loop expectation value, which in turn has been found to agree with the magnetisation critical exponent $\frac{1}{9}$ of the two-dimensional $q = 3$ Potts model [46]. It would be interesting to investigate this relation further, although this requires numerical simulations close to the phase transition, where they are known to be difficult.

Once the mobility edge is known, the density of localised modes in physical units can be computed as

$$\frac{\mathcal{N}_{\text{loc}}}{V_{\text{phys}}} = \frac{\mathcal{N}_{\text{loc}} \bar{\beta}^2}{V} = \left(\frac{\bar{\beta}}{N_s}\right)^2 \int_0^{\lambda_c} d\lambda \rho(\lambda), \quad (4.10)$$

where both λ and the spectral density $\rho(\lambda) = \langle \sum_n \delta(\lambda - \lambda_n) \rangle$ are in lattice units. In Fig. 13 I show this quantity multiplied by $T/\lambda_{c\text{phys}} = 1/(N_t \lambda_c)$, i.e.,

$$R \equiv \frac{\mathcal{N}_{\text{loc}} T}{V_{\text{phys}} \lambda_{c\text{phys}}} = \left(\frac{\bar{\beta}}{N_s}\right)^2 \frac{1}{\lambda_c N_t} \int_0^{\lambda_c} d\lambda \rho(\lambda). \quad (4.11)$$

This quantity is independent of temperature within errors, and a simple constant fit gives¹⁶ $R = 0.642(85)$. This means that the density of localised modes behaves like $\mathcal{N}_{\text{loc}}/V_{\text{phys}} \propto \lambda_{c\text{phys}}/T \simeq (T - T_c)^v/T$, with $T_c = \bar{\beta}_c/N_t$, and since $v \sim 0.1 \div 0.2$ one has that it rises steeply to a maximum, and then decreases quite fast with temperature. This is different from what was found in QCD in 3+1 dimensions [16]: there, the density of localised modes was seen to keep increasing, up to the highest available temperatures of about $5T_c$, while here the decrease begins already at $1.1 \div 1.2T_c$.

To conclude the discussion of spectral statistics, I present an independent test, usually referred to as *shape analysis* [68], for the one-parameter scaling hypothesis, Eq. (3.8), exploited above to determine the mobility edge by means of a finite-size scaling analysis. If indeed a single quantity, namely the ratio $\log \xi / \log L$, determines the statistical properties of the spectrum, then plotting one spectral statistic against another should yield universal curves, on which the data points coming from different volumes and lattice couplings should all (approximately) lie, at least for sufficiently large volumes. In Fig. 14 I show plots of $\langle s^2 \rangle_\lambda$ against I_λ in the deconfined phase for $N_s = 64, 72$. Only points for which $|\langle s \rangle_\lambda - 1| < 0.05$ are plotted. Data from different lattice couplings lie on a common curve connecting the RMT point and the Poisson point. The same kind of behaviour has been observed in 3+1-dimensional QCD [67, 69]. The dashed line corresponds to the statistics determined by the so-called “sinh-kernel”,¹⁷ a one-parameter family of two-level connected correlators that describes the statistical behaviour in the bulk of the spectrum for several different random matrix models [70–72]. This curve runs close to the numerical data obtained in 3+1 dimensional QCD, intersecting them at the critical point [67]. In the present case, this curve describes well the numerical data close to the RMT point, up to (and possibly even beyond) the critical points found for the different values of the lattice coupling. This suggests that the spectral statistics on the line of critical points above the mobility edge belong to the family parameterised by the sinh-kernel. Numerical errors are however still too large to make conclusive statements.

After this long discussion of the high-temperature phase, a few words about the low-temperature phase are in order. In Fig. 15 I show the spectral statistics I_λ and $\langle s^2 \rangle_\lambda$ in the confined phase. Analogously to what was found for the fractal dimension of the eigenmodes, the spectral statistics do not show a uniform RMT-type behaviour, but they get closer to Poisson behaviour in the low end of the spectrum, the more so as one gets closer to the deconfinement transition. The transition in the spectrum however does not seem to be a genuine phase transition: the distance from Poisson behaviour remains large even for the largest volumes (as can be seen in the shape-analysis plot in Fig. 16), and attempts at an unconstrained finite-size scaling analysis fail. It is likely that in the infinite-volume limit the spectral statistics converge to a non-trivial behaviour interpolating between Poisson and RMT: this would reflect the non-trivial fractal dimension of the eigenmodes.¹⁸

¹⁶Reinstating powers of g^2 , one has $R = 0.642(85) (g^2/2)^2$.

¹⁷I thank F. Pittler for evaluating numerically the relevant quantities.

¹⁸Notice that what is being discussed here are bulk spectral statistics near the origin, and not microscopic spectral statistics, which require a different type of unfolding (see, e.g., Ref. [40]). For a comparison between

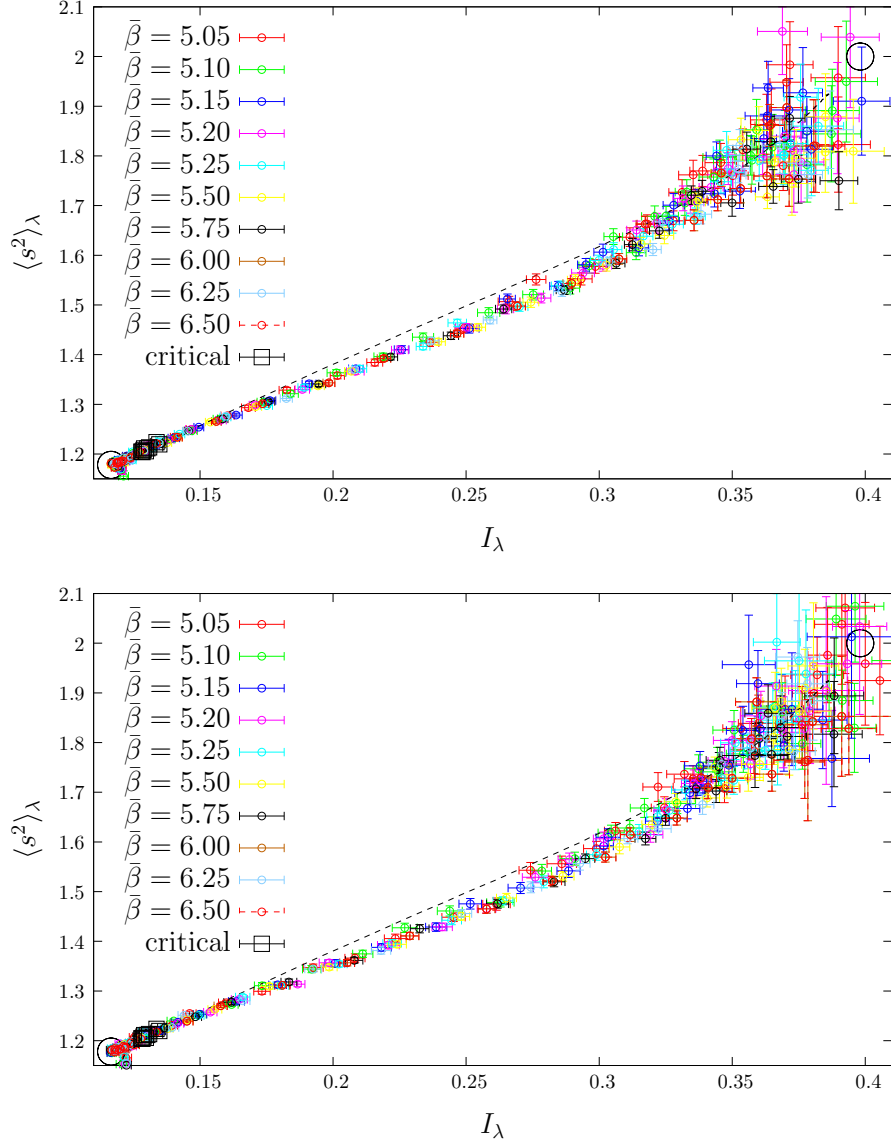


Figure 14. Shape analysis. Each data point corresponds to the pair $(I_\lambda, \langle s^2 \rangle_\lambda)$ associated to the same point λ in the spectrum. The pairs corresponding to the mobility edges for the various couplings are shown as black squares. In the top panel $N_s = 64$, while in the bottom panel $N_s = 72$. Results for different lattice couplings and different volumes all lie approximately on the same curve. The points corresponding to RMT and Poisson statistics are denoted with circles. The curve corresponding to the sinh-kernel is shown with a dashed line.

Combining the behaviour of the spectral statistics observed in the confined phase with that observed at the mobility edge in the deconfined phase, one is led to conjecture the following development with temperature. The spectral statistics at the low end of the spectrum

the RMT predictions for the microscopic statistics and lattice data (at zero temperature) cf. Ref. [73].

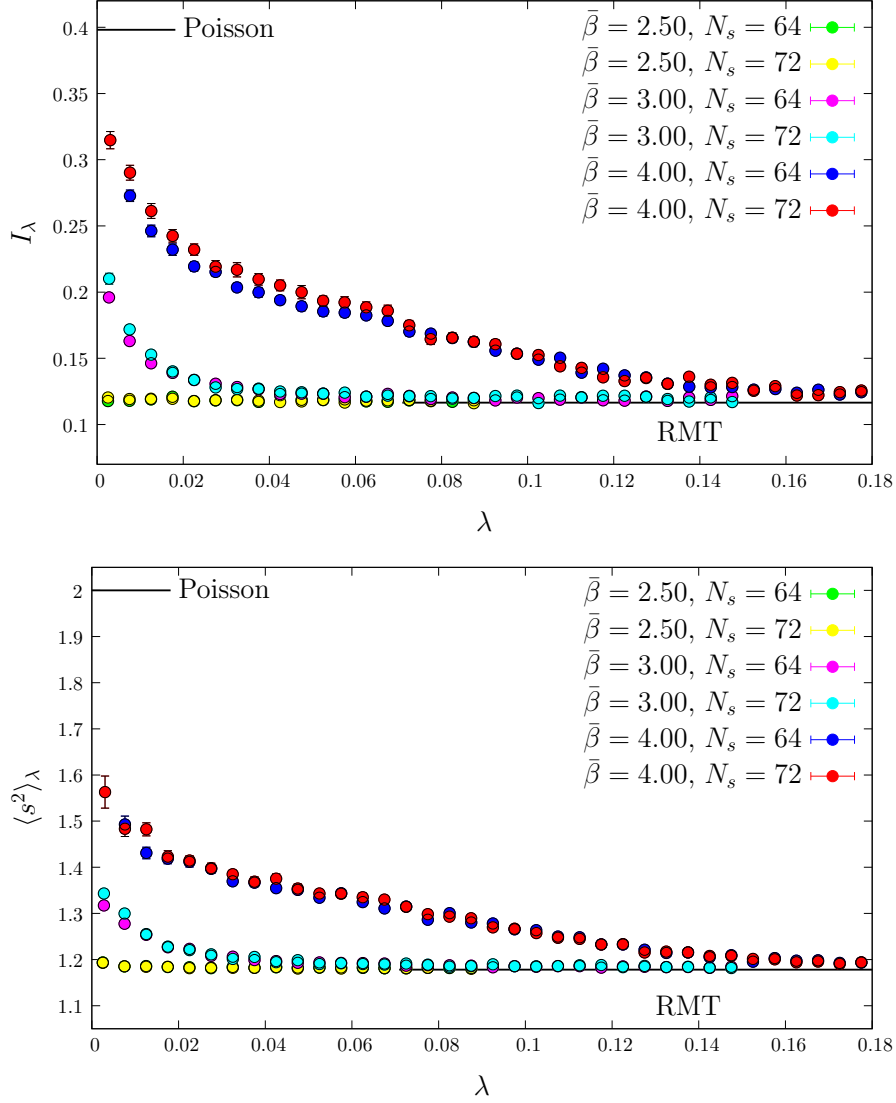


Figure 15. Spectral statistics I_λ (top) and $\langle s^2 \rangle_\lambda$ (bottom) in the confined phase, for the two largest lattice sizes.

keeps approaching the Poisson statistics as the deconfinement transition is approached from below, and reaches it at the critical lattice coupling. At the same time, the crossover along the spectrum turns into a true BKT-type, localisation/delocalisation phase transition, and a mobility edge appears at the origin. Moving further into the deconfined phase, the mobility edge moves up in the spectrum and the statistics at the mobility edge moves towards RMT, apparently stabilising at an intermediate point between Poisson and RMT for sufficiently large temperature.

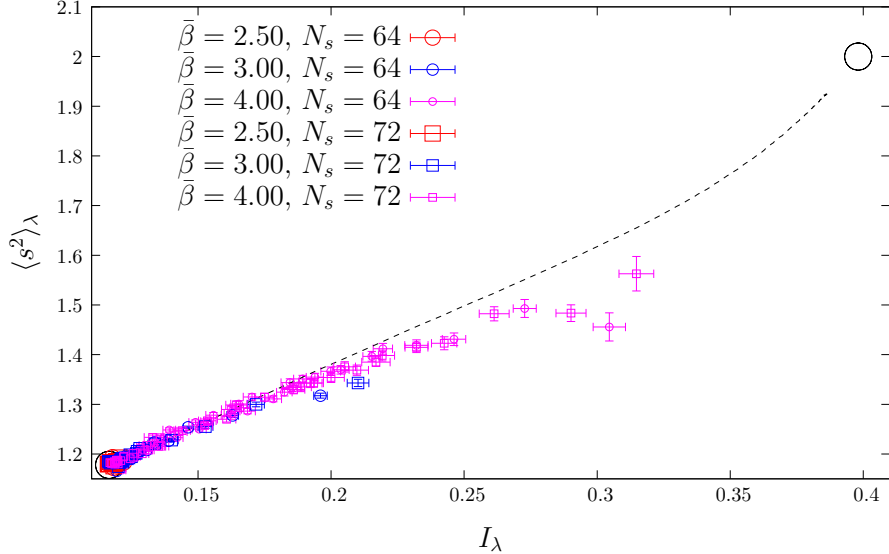


Figure 16. Shape analysis in the low-temperature phase. Only points with $|\langle s \rangle_\lambda - 1| < 0.1$ are included.

5 Conclusions and outlook

The connection between deconfinement, chiral symmetry restoration and localisation of the low Dirac modes has become increasingly evident in recent years, both in QCD [12–14, 16–19, 44] and in QCD-like theories [15, 22–25]. The theoretical arguments of Refs. [25–27] suggest that the driving force behind both chiral symmetry restoration and localisation is the ordering of the Polyakov lines causing deconfinement. This is further supported by numerical studies of dedicated toy models [25]. Given the generality of these arguments, the connection between these three phenomena is expected to be of rather general nature.

A non-trivial test of this idea has been provided in the present paper, devoted to the study of localisation of Dirac modes in 2+1 dimensional SU(3) pure gauge theory at finite temperature on the lattice. This model differs from QCD and from the other QCD-like models mentioned above in several aspects: different dimensionality (2+1 instead of 3+1), different critical behaviour at deconfinement (second-order phase transition instead of crossover or first order),¹⁹ different expected type of localisation/delocalisation transition (BKT instead of second order). While the simultaneity of deconfinement and chiral restoration has long been known [4], no previous studies existed about localisation of the Dirac modes. The numerical results presented here, obtained with the staggered discretisation, indicate that the lowest Dirac modes are delocalised (although with non-trivial fractal dimension) in the confined phase, and localised in the deconfined phase. A BKT-type Anderson transition is seen to take place at a critical point (mobility edge) in the spectrum in the high-temperature

¹⁹The only exception is the SU(2) case studied in Ref. [15], where however no detailed study of the transition region was made.

phase, in agreement with expectations based on universality arguments and on known results for the two-dimensional unitary Anderson model [30]. Although this is perfectly natural in the framework of the Dirac-Anderson approach [25], it is by itself a rather nontrivial finding, which provides nontrivial support to the related sea/islands mechanism [26, 27] for localisation in high-temperature gauge theories. Both the inverse of the typical size of localised modes and the mobility edge extrapolate to zero at temperatures compatible with the deconfinement temperature, as determined in Ref. [49], indicating that the onset of localisation coincides with deconfinement and chiral symmetry restoration. This work thus provides further support to the idea of deconfinement driving the system to a chirally restored phase with localised low Dirac modes.

There are other theories where it would be worth studying the relation between deconfinement, chiral symmetry restoration and localisation. The case of gauge theories in the presence of an imaginary chemical potential is interesting both for its theoretical aspects, and for the possible relevance to the study of hadronic matter at finite density. Since the imaginary chemical potential changes the effective boundary conditions affecting the Dirac eigenmodes, according to the sea/islands picture and the Dirac-Anderson approach it should control the density and the localisation properties of the low modes. Preliminary results [36] show that in $SU(3)$ pure gauge theory in 2+1 dimensions an imaginary chemical potential leads to an increase both in the spectral density near the origin and in the size of the low modes, eventually leading to chiral-symmetry breaking and delocalisation of the low modes for sufficiently large imaginary chemical potential, in agreement with expectations.

Another interesting case is that of $U(1)$ pure gauge theory in 2+1 dimensions, for various reasons. The Abelian nature of the gauge group and the different nature (BKT) of the finite-temperature deconfining transition provide a setup qualitatively different from any other investigated so far. Moreover, in contrast with the case of $SU(N_c)$ gauge groups, in the high-temperature phase there is no infinite barrier in the thermodynamic limit separating Polyakov loop sectors that differ by the phase of the spatially-averaged Polyakov loop. Since it is the phases of the Polyakov lines that provide the effective boundary conditions for the Dirac modes, in turn determining their localisation properties, one expects the coexistence of localised and delocalised modes at the low end of the spectrum. Also in this case the available preliminary results [36] confirm the expectations.

An important consequence of localisation of the low modes is that it prevents a spontaneously broken continuous symmetry from generating Goldstone bosons [74, 75]. If the low Dirac modes become localised at deconfinement then the Goldstone mechanism does not apply anymore, independently of the spectral density near the origin, and Goldstone bosons disappear from the spectrum. From this point of view, the connection between deconfinement and localisation is possibly even more important than that between localisation and chiral symmetry breaking. A setting in which these issues can be investigated is the $SU(3)$ gauge theory with adjoint fermions in 3+1 dimensions, which has long been known to display separate deconfining and chirally-restoring phase transitions [9]. Preliminary (unpublished) results show that this happens also in 2+1 dimensions with gauge group $SU(2)$ in the quenched

approximation, and that while the spectral density remains finite above the deconfinement transition, the near-zero modes become localised.

The results of these paper increase the confusion about the role played by topology in making the low Dirac modes localised. In Refs. [12, 13] the localised modes were understood as coming from the localised zero modes supported by instantons at finite temperature. However, the authors of Ref. [15] claimed that the estimated density of topological objects was an order of magnitude smaller than that of localised modes (in quenched SU(2) configurations). More recently, in Ref. [22] (see also Ref. [76]) the density of topological near-zero modes in the pure gauge SU(3) theory was shown to account only up to 60% of the localised modes at the deconfinement transition, a fraction rapidly falling with temperature, and which overestimates the corresponding result in the presence of dynamical fermions. The results of Ref. [17] (for QCD with domain-wall fermions) show that localised modes prefer locations with larger action density and topological charge density, which may be related to the positions of L - \bar{L} monopole-instanton pairs. On the other hand, in 2+1 dimensions there is no topological charge for SU(3) fields, since the homotopy group $\pi_2(\text{SU}(3))$ is trivial, and nonetheless localised modes appear in the deconfined phase. Further studies are needed to clarify this issue, which, given the close relation between localisation and deconfinement, might even help in understanding the role played by topology in the deconfinement transition.

In conclusion, further studies of localisation in gauge theories may help in better understanding the relation between confinement and chiral symmetry breaking.

Acknowledgements

I wish to thank M. Caselle, J. Greensite, D. Nógrádi, F. Pittler and L. von Smekal for useful discussions, and T. G. Kovács both for discussions and for a careful reading of the manuscript. This work was partly supported by grants OTKA-K-113034 and NKFIH-KKP126769.

References

- [1] WUPPERTAL-BUDAPEST collaboration, *Is there still any T_c mystery in lattice QCD? Results with physical masses in the continuum limit III*, *JHEP* **09** (2010) 073 [[1005.3508](#)].
- [2] A. Bazavov, N. Brambilla, H. T. Ding, P. Petreczky, H. P. Schadler, A. Vairo et al., *Polyakov loop in 2+1 flavor QCD from low to high temperatures*, *Phys. Rev.* **D93** (2016) 114502 [[1603.06637](#)].
- [3] G. Boyd, J. Engels, F. Karsch, E. Laermann, C. Legeland, M. Lütgemeier et al., *Thermodynamics of SU(3) lattice gauge theory*, *Nucl. Phys.* **B469** (1996) 419 [[hep-lat/9602007](#)].
- [4] P. H. Damgaard, U. M. Heller, A. Krasnitz and T. Madsen, *A quark-anti-quark condensate in three-dimensional QCD*, *Phys. Lett.* **B440** (1998) 129 [[hep-lat/9803012](#)].
- [5] F. Karsch, E. Laermann and C. Schmidt, *The chiral critical point in three-flavor QCD*, *Phys. Lett.* **B520** (2001) 41 [[hep-lat/0107020](#)].

- [6] P. de Forcrand and O. Philipsen, *The QCD phase diagram for three degenerate flavors and small baryon density*, *Nucl. Phys.* **B673** (2003) 170 [[hep-lat/0307020](#)].
- [7] P. de Forcrand and O. Philipsen, *The chiral critical point of $N_f = 3$ QCD at finite density to the order $(\mu/T)^4$* , *JHEP* **11** (2008) 012 [[0808.1096](#)].
- [8] G. Bergner, C. López and S. Piemonte, *A study of center and chiral symmetry realization in thermal $\mathcal{N} = 1$ super Yang-Mills theory using the gradient flow*, [1902.08469](#).
- [9] F. Karsch and M. Lütgemeier, *Deconfinement and chiral symmetry restoration in an $SU(3)$ gauge theory with adjoint fermions*, *Nucl. Phys.* **B550** (1999) 449 [[hep-lat/9812023](#)].
- [10] T. DeGrand, Y. Shamir and B. Svetitsky, *Near the Sill of the Conformal Window: Gauge Theories with Fermions in Two-Index Representations*, *Phys. Rev.* **D88** (2013) 054505 [[1307.2425](#)].
- [11] T. Banks and A. Casher, *Chiral symmetry breaking in confining theories*, *Nucl. Phys.* **B169** (1980) 103.
- [12] A. M. García-García and J. C. Osborn, *Chiral phase transition and Anderson localization in the Instanton Liquid Model for QCD*, *Nucl. Phys.* **A770** (2006) 141 [[hep-lat/0512025](#)].
- [13] A. M. García-García and J. C. Osborn, *Chiral phase transition in lattice QCD as a metal-insulator transition*, *Phys. Rev.* **D75** (2007) 034503 [[hep-lat/0611019](#)].
- [14] T. G. Kovács, *Absence of correlations in the QCD Dirac spectrum at high temperature*, *Phys. Rev. Lett.* **104** (2010) 031601 [[0906.5373](#)].
- [15] T. G. Kovács and F. Pittler, *Anderson Localization in Quark-Gluon Plasma*, *Phys. Rev. Lett.* **105** (2010) 192001 [[1006.1205](#)].
- [16] T. G. Kovács and F. Pittler, *Poisson-random matrix transition in the QCD Dirac spectrum*, *Phys. Rev.* **D86** (2012) 114515 [[1208.3475](#)].
- [17] G. Cossu and S. Hashimoto, *Anderson Localization in high temperature QCD: background configuration properties and Dirac eigenmodes*, *JHEP* **06** (2016) 056 [[1604.00768](#)].
- [18] L. Holicki, E.-M. Ilgenfritz and L. von Smekal, *The Anderson transition in QCD with $N_f = 2 + 1 + 1$ twisted mass quarks: overlap analysis*, [1810.01130](#).
- [19] M. Giordano, T. G. Kovács and F. Pittler, *Universality and the QCD Anderson Transition*, *Phys. Rev. Lett.* **112** (2014) 102002 [[1312.1179](#)].
- [20] P. A. Lee and T. V. Ramakrishnan, *Disordered electronic systems*, *Rev. Mod. Phys.* **57** (1985) 287.
- [21] F. Evers and A. D. Mirlin, *Anderson transitions*, *Rev. Mod. Phys.* **80** (2008) 1355 [[0707.4378](#)].
- [22] T. G. Kovács and R. A. Vig, *Localization transition in $SU(3)$ gauge theory*, *Phys. Rev.* **D97** (2018) 014502 [[1706.03562](#)].
- [23] M. Giordano, S. D. Katz, T. G. Kovács and F. Pittler, *Deconfinement, chiral transition and localisation in a QCD-like model*, *JHEP* **02** (2017) 055 [[1611.03284](#)].
- [24] M. Giordano, T. G. Kovács and F. Pittler, *Localization and chiral properties near the ordering transition of an Anderson-like toy model for QCD*, *Phys. Rev.* **D95** (2017) 074503 [[1612.05059](#)].

- [25] M. Giordano, T. G. Kovács and F. Pittler, *An Anderson-like model of the QCD chiral transition*, *JHEP* **06** (2016) 007 [[1603.09548](#)].
- [26] F. Bruckmann, T. G. Kovács and S. Schierenberg, *Anderson localization through Polyakov loops: Lattice evidence and random matrix model*, *Phys. Rev.* **D84** (2011) 034505 [[1105.5336](#)].
- [27] M. Giordano, T. G. Kovács and F. Pittler, *An Ising-Anderson model of localisation in high-temperature QCD*, *JHEP* **04** (2015) 112 [[1502.02532](#)].
- [28] R. D. Pisarski, *Chiral-symmetry breaking in three-dimensional electrodynamics*, *Phys. Rev.* **D29** (1984) 2423.
- [29] C. Burden and A. N. Burkitt, *Lattice Fermions in Odd Dimensions*, *Europhys. Lett.* **3** (1987) 545.
- [30] X. C. Xie, X. R. Wang and D. Z. Liu, *Kosterlitz-Thouless-type metal-insulator transition of a 2D electron gas in a random magnetic field*, *Phys. Rev. Lett.* **80** (1998) 3563.
- [31] P. W. Anderson, *Absence of Diffusion in Certain Random Lattices*, *Phys. Rev.* **109** (1958) 1492.
- [32] P. de Forcrand, *Localization properties of fermions and bosons*, *AIP Conf. Proc.* **892** (2007) 29 [[hep-lat/0611034](#)].
- [33] D. Diakonov and V. Yu. Petrov, *A Theory of Light Quarks in the Instanton Vacuum*, *Nucl. Phys.* **B272** (1986) 457.
- [34] D. Diakonov, *Chiral symmetry breaking by instantons*, *Proc. Int. Sch. Phys. Fermi* **130** (1996) 397 [[hep-ph/9602375](#)].
- [35] A. M. Halász and J. J. M. Verbaarschot, *Universal fluctuations in spectra of the lattice Dirac operator*, *Phys. Rev. Lett.* **74** (1995) 3920 [[hep-lat/9501025](#)].
- [36] M. Giordano, *Localisation, chiral symmetry and confinement in QCD and related theories*, [1811.04792](#).
- [37] B. L. Altshuler and B. I. Shklovskii, *Repulsion of energy levels and conductivity of small metal samples*, *Sov. Phys. JETP* **64** (1986) 127.
- [38] M. L. Mehta, *Random matrices*, vol. 142. Elsevier, 3 ed., 2004.
- [39] T. Guhr, A. Müller-Groeling and H. A. Weidenmüller, *Random matrix theories in quantum physics: Common concepts*, *Phys. Rept.* **299** (1998) 189 [[cond-mat/9707301](#)].
- [40] J. J. M. Verbaarschot and T. Wettig, *Random matrix theory and chiral symmetry in QCD*, *Ann. Rev. Nucl. Part. Sci.* **50** (2000) 343 [[hep-ph/0003017](#)].
- [41] M. R. Zirnbauer, *Symmetry Classes*, in *The Oxford Handbook of Random Matrix Theory*, G. Akemann, J. Baik and P. Di Francesco, eds., pp. 43–65, Oxford University Press, (2011), [1001.0722](#).
- [42] B. I. Shklovskii, B. Shapiro, B. R. Sears, P. Lambrianides and H. B. Shore, *Statistics of spectra of disordered systems near the metal-insulator transition*, *Phys. Rev.* **B47** (1993) 11487.
- [43] K. Slevin and T. Ohtsuki, *Corrections to scaling at the Anderson transition*, *Phys. Rev. Lett.* **82** (1999) 382 [[cond-mat/9812065](#)].

- [44] L. Ujfalusi, M. Giordano, F. Pittler, T. G. Kovács and I. Varga, *Anderson transition and multifractals in the spectrum of the Dirac operator of Quantum Chromodynamics at high temperature*, *Phys. Rev.* **D92** (2015) 094513 [[1507.02162](#)].
- [45] M. Gross and J. F. Wheeler, *Deconfining Transitions in (2+1)-dimensional SU(3) and SU(4) Gauge Theories*, *Z. Phys.* **C28** (1985) 471.
- [46] J. Christensen, G. Thorleifsson, P. H. Damgaard and J. F. Wheeler, *Thermodynamics of SU(3) lattice gauge theory in (2+1)-dimensions*, *Nucl. Phys.* **B374** (1992) 225.
- [47] J. Christensen, G. Thorleifsson, P. H. Damgaard and J. F. Wheeler, *Three-dimensional deconfinement transitions and conformal symmetry*, *Phys. Lett.* **B276** (1992) 472.
- [48] J. Engels, F. Karsch, E. Laermann, C. Legeland, M. Lutgemeier, B. Petersson et al., *A study of finite temperature gauge theory in (2+1)-dimensions*, *Nucl. Phys. Proc. Suppl.* **53** (1997) 420 [[hep-lat/9608099](#)].
- [49] J. Liddle and M. Teper, *The deconfining phase transition in D=2+1 SU(N) gauge theories*, [0803.2128](#).
- [50] P. Bialas, L. Daniel, A. Morel and B. Petersson, *Thermodynamics of SU(3) Gauge Theory in 2 + 1 Dimensions*, *Nucl. Phys.* **B807** (2009) 547 [[0807.0855](#)].
- [51] P. Bialas, L. Daniel, A. Morel and B. Petersson, *Three dimensional finite temperature SU(3) gauge theory in the confined region and the string picture*, *Nucl. Phys.* **B836** (2010) 91 [[0912.0206](#)].
- [52] P. Bialas, L. Daniel, A. Morel and B. Petersson, *Three dimensional finite temperature SU(3) gauge theory near the phase transition*, *Nucl. Phys.* **B871** (2013) 111 [[1211.3304](#)].
- [53] E. N. Economou and P. D. Antoniou, *Localization and off-diagonal disorder*, *Solid State Commun.* **21** (1977) 285.
- [54] D. Weaire and V. Srivastava, *Numerical results for Anderson localisation in the presence of off-diagonal disorder*, *Solid State Commun.* **23** (1977) 863.
- [55] V. L. Berezinskiĭ, *Destruction of long range order in one-dimensional and two-dimensional systems having a continuous symmetry group. I. Classical systems*, *Sov. Phys. JETP* **32** (1971) 493.
- [56] V. L. Berezinskiĭ, *Destruction of long-range order in one-dimensional and two-dimensional systems possessing a continuous symmetry group. II. Quantum systems*, *Sov. Phys. JETP* **34** (1971) 610.
- [57] J. M. Kosterlitz and D. J. Thouless, *Ordering, metastability and phase transitions in two-dimensional systems*, *J. Phys.* **C6** (1973) 1181.
- [58] M. N. Barber, *Finite-size scaling*, in *Phase transitions and critical phenomena*, C. Domb and J. L. Lebowitz, eds., vol. 8, (London), pp. 146–266, Academic Press, (1983).
- [59] E. Abrahams, P. W. Anderson, D. C. Licciardello and T. V. Ramakrishnan, *Scaling theory of localization: Absence of quantum diffusion in two dimensions*, *Phys. Rev. Lett.* **42** (1979) 673.
- [60] R. B. Lehoucq, D. C. Sorensen and C. Yang, *ARPACK users' guide: solution of large-scale eigenvalue problems with implicitly restarted Arnoldi methods*, vol. 6. Siam, 1998.
- [61] M. Creutz, *Monte Carlo Study of Quantized SU(2) Gauge Theory*, *Phys. Rev.* **D21** (1980) 2308.

- [62] N. Cabibbo and E. Marinari, *A New Method for Updating $SU(N)$ Matrices in Computer Simulations of Gauge Theories*, *Phys. Lett.* **119B** (1982) 387.
- [63] F. R. Brown and T. J. Woch, *Overrelaxed Heat Bath and Metropolis Algorithms for Accelerating Pure Gauge Monte Carlo Calculations*, *Phys. Rev. Lett.* **58** (1987) 2394.
- [64] M. Creutz, *Overrelaxation and Monte Carlo Simulation*, *Phys. Rev.* **D36** (1987) 515.
- [65] F. James and M. Roos, *Minuit: A System for Function Minimization and Analysis of the Parameter Errors and Correlations*, *Comput. Phys. Commun.* **10** (1975) 343.
- [66] G. P. Lepage, B. Clark, C. T. H. Davies, K. Hornbostel, P. B. Mackenzie, C. Morningstar et al., *Constrained curve fitting*, *Nucl. Phys. Proc. Suppl.* **106** (2002) 12 [[hep-lat/0110175](#)].
- [67] S. M. Nishigaki, M. Giordano, T. G. Kovács and F. Pittler, *Critical statistics at the mobility edge of QCD Dirac spectra*, *PoS LATTICE2013* (2014) 018 [[1312.3286](#)].
- [68] I. Varga, E. Hofstetter, M. Schreiber and J. Pipek, *Shape analysis of the level-spacing distribution around the metal-insulator transition in the three-dimensional Anderson model*, *Phys. Rev. B* **52** (1995) 7783 [[cond-mat/9407058](#)].
- [69] M. Giordano, T. G. Kovács and F. Pittler, *Anderson localization in QCD-like theories*, *Int. J. Mod. Phys.* **A29** (2014) 1445005 [[1409.5210](#)].
- [70] K. A. Muttalib, Y. Chen, M. E. H. Ismail and V. N. Nicopoulos, *New family of unitary random matrices*, *Phys. Rev. Lett.* **71** (1993) 471.
- [71] A. D. Mirlin, Y. V. Fyodorov, F.-M. Dittes, J. Quezada and T. H. Seligman, *Transition from localized to extended eigenstates in the ensemble of power-law random banded matrices*, *Phys. Rev.* **E54** (1996) 3221 [[cond-mat/9604163](#)].
- [72] M. Moshe, H. Neuberger and B. Shapiro, *A generalized ensemble of random matrices*, *Phys. Rev. Lett.* **73** (1994) 1497.
- [73] P. Bialas, Z. Burda and B. Petersson, *Random matrix model for QCD₃ staggered fermions*, *Phys. Rev.* **D83** (2011) 014507 [[1006.0360](#)].
- [74] A. J. McKane and M. Stone, *Localization as an alternative to Goldstone's theorem*, *Annals Phys.* **131** (1981) 36.
- [75] M. Golterman and Y. Shamir, *Localization in lattice QCD*, *Phys. Rev.* **D68** (2003) 074501 [[hep-lat/0306002](#)].
- [76] T. G. Kovács and R. A. Vig, *Localization and topology in high temperature QCD*, [1901.00661](#).